Mircea Vicențiu Săceleanu

Mario Monzon Ilaria Cacciotti

Iulian Antoniac

Brain Revealed

Handbook for Students and Practitioners

Vol. I

Editura Universității „Lucian Blaga“ din Sibiu

2021

Descrierea CIP a Bibliotecii Naţionale a României
Brain reveal : hadbook for students and practitioners / coord.: Mircea Vicenţiu Săceleanu. - Sibiu : Editura Universităţii "Lucian Blaga" din Sibiu, 2021
2 vol.
ISBN 978-606-12-1860-8
Vol. 1. - 2021. - Conţine bibliografie. - ISBN 978-606-12-1861-5

I. Săceleanu, Vicenţiu Mircea (coord.)

616.8

Co-funded by the Erasmus+ Programme of the European Union

CASES STUDIES OF TRAINING MATERIAL APPLIED TO NEUROSURGERY

Rubén Paz[1],
Mario Monzón[1],
Joshua García[1]
Yamilet Rivero[1]

[1] Department of Mechanical Engineering, Campus de Tafira Baja, Edificio de Ingenierías, University of Las Palmas de Gran Canaria, 35017, Las Palmas, Spain

This chapter explains all the process steps carried out to produce several synthetic models from real cases of cranial trauma, brain tumor and cerebral aneurysm. The synthetic models were mainly produced by Additive Manufacturing (AM) technologies, but also combined with conventional manufacturing processes such as silicone molding. The combination of AM (material extrusion technologies) and conventional techniques, together with the correct selection of materials, made possible to produce realistic synthetic models from the real scan data with low-cost approaches.

Contents

1.1. Training material for surgery of cranial trauma

The first summer school of the BrainIT project (July 2019) focused on trauma in neurosurgery. Two cases were developed for the practical sessions of this summer school:

- An intracranial hematoma with large skull fracture
- An intracranial hematoma, without skull fracture

Both cases were developed starting from the real scanning images of the patients and with low-cost manufacturing approaches. Material extrusion AM was used to produce 10 replicas of each case for the practical training sessions. In both cases, the students had to cut the skull in the correct area, remove the hematoma by vacuum and place/sew again the removed bone.

As the 3D printed models would be produced by material extrusion AM, the first step was to select the best 3D printable filament to mimic the properties of the skull. Among the possibilities, two main materials were considered: polylactic acid (PLA) and Smartfil® EP, which is a mixture of 30% of calcium carbonate ($CaCO_3$) and 70% of PLA. The PLA filament was selected as it is the most common plastic for material extrusion AM due to its outstanding printability. On the other hand, the EP filament was chosen due to its content in calcium carbonate, which is also present in bones and, consequently, could provide similar properties to the real bone.

To compare both materials, different tests were carried out in terms of flexural mechanical properties, drilling/milling cutting forces and chips behavior, surface hardness and the validation of a neurosurgeon.

The first analysis consisted in a flexural mechanical test. Five standard samples of each material were 3D printed and tested under three-point flexural test according to ISO 178 in a universal testing machine (Figure 1).

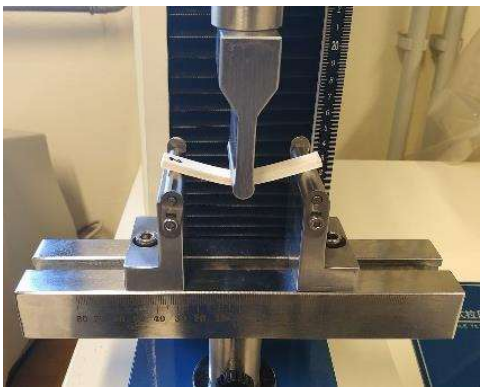

Figure 17. Three-point flexural tests on 3D printed specimens.

The results showed that the EP samples had a more fragile behavior, with higher elastic modulus (3389.46 MPa) than PLA (2743.51 MPa) and lower flexural strength (71.42 MPa) than PLA (93.53 MPa). Figure 18 represents a simplification of the flexural behavior of both materials, using the elastic modulus as the slope of the linear elastic zone until the yield point, and defining another linear behavior in the plastic zone until the point of maximum strength.

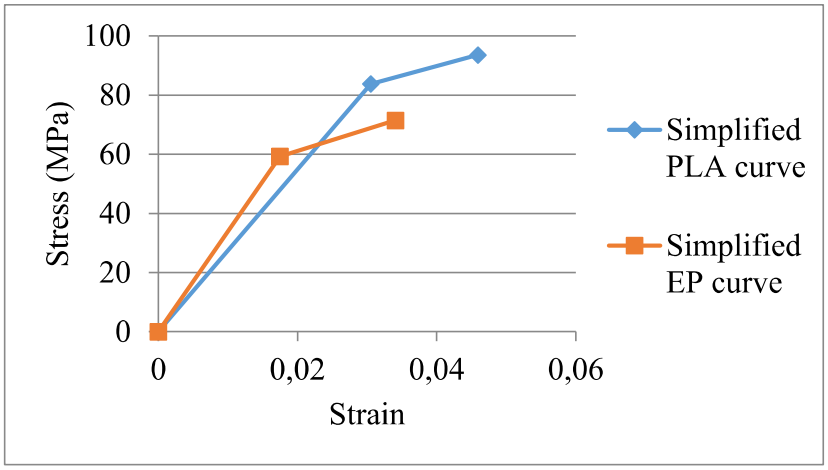

Figure 18. Simplified representative behavior of 3D printed PLA and EP under flexural loads.

According to the literature [1]–[4], the average flexural elastic modulus of the skull bone is around 9625 MPa and the flexural strength around 106.48 MPa (average values obtained from the previous references). As a conclusion, the presence of $CaCO_3$ increases the elastic modulus of EP filament (which is closer to the real bone, although still not close) and reduces the flexural strength.

The behavior of these materials during drilling and milling was also compared, but in this case also testing a cow bone to have an approximated reference value. In the case of the drilling, a load cell was installed under the specimens and the forces during the drilling were registered. The same drilling conditions were applied (4.5 mm diameter drill bit, 10 mm/min feed rate, 2000 rpm rotational speed and 10 mm depth) in four drillings of each material. Figure 19 shows one of the tests on the reference bone and Figure 20 the resulting bone with the 4 drills.

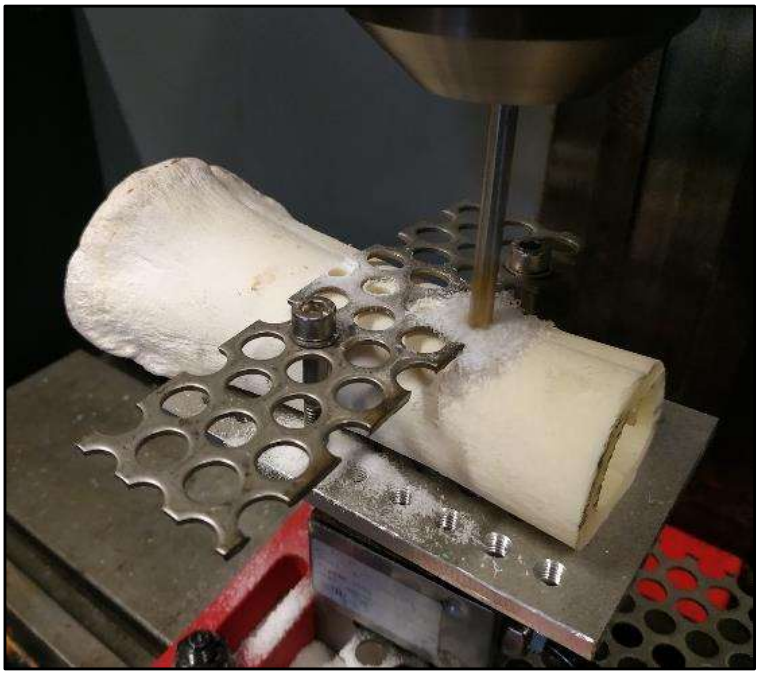

Figure 19. Cutting force measurement during drilling (in a reference bone).

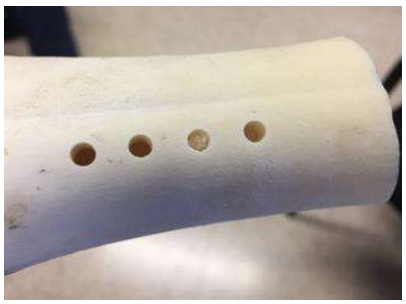

Figure 20. Reference bone after the drilling tests.

The average force-time curves of the 3 materials are depicted in Figure 21. The maximum cutting force during drilling was quite similar between EP material and bone. However, in PLA the drilling forces were higher.

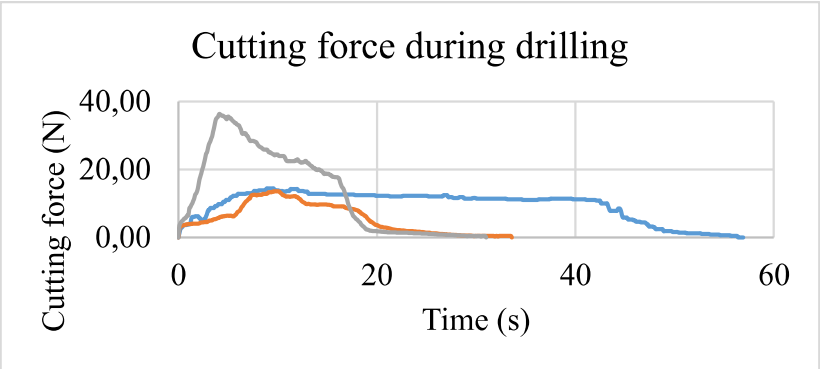

Figure 21. Cutting force during drilling in the different materials tested (blue: bone; orange: EP; grey: PLA). The maximum drilling force is almost the same in the case of EP and bone, while in PLA was higher.

For the milling test, the load cell was placed in the lateral side of the holder of the specimens (Figure 22), so that the milling tool feed rate was towards the load cell. The same milling conditions were applied for all the materials (mill tool of 4 mm diameter, 50 mm/min feed rate, 2000 rpm rotational speed, and 2 mm depth) and the resulting average curve of five millings (force-time) was calculated, as depicted in Figure 23. The

results showed that the milling forces were lower in EP material, while PLA and boner had similar values.

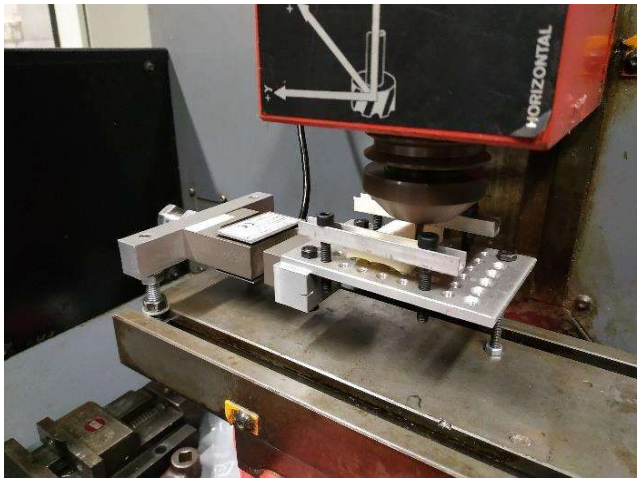

Figure 22. Cutting force measurement during milling.

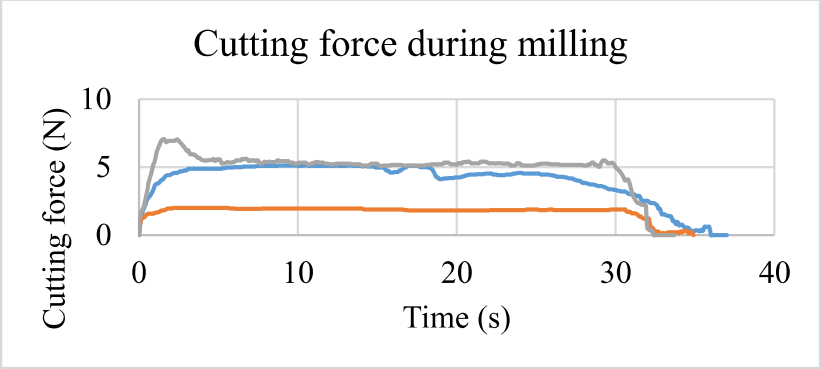

Figure 23. Cutting force during milling in the different materials tested (blue: bone; orange: EP; grey: PLA). In the case of milling, EP obtained lower values compared to PLA and real bone.

Regarding the behavior of the chips during milling and drilling, it was observed that small chips and powder were removed in the case of the bone. However, in the PLA specimens, the material tended to melt

and stick to the tool (both in drilling and milling), while in the case of EP, the behavior was more similar to the real bone (although in some cases the material also tended to melt).

With regard to the surface hardness, the Shore D hardness was measured in five tests for each material. The results showed that the hardness was relatively similar in all the cases, with an average value of 82 for PLA, 83 for EP and 77 for the bone (Shore D).

In general, the EP filament performed better than PLA. For this reason, a skull sample was manufactured with the EP filament for the validation of an experienced neurosurgeon. The neurosurgeon did some practical verification cutting the skull and validated the material with a positive feedback. Table 4 summarizes the results of the comparison between PLA and EP materials.

Table 4. Comparison of EP and PLA under the different criteria evaluated.

Analyzed criterion	**Smartfil® EP**	**PLA (without additives)**
Flexural elastic modulus	☒	☒
Flexural strength	☒	☒
Maximum drilling cutting force	☒	☒
Maximum milling cutting force	☒	☒
Chips behavior	☒	☒
Hardness (Shore D)	☒	☒
Neurosurgeon's validation	☒	☒

Regarding the hematoma material, after different tests with different concentrations, the final choice was a solution of sodium

alginate powder (from Acros Organics) with distilled water (1:20 w/w) (Figure 40). This solution was also approved by the surgeon to simulate the hematoma.

1.1.1. Case 1: Intracranial hematoma (with skull fracture)

The first case was an intracranial hematoma with skull fracture (the patient suffered a severe trauma with a large fracture).

Once selected the material for the skull and hematoma, the 3D reconstruction was made by using the CT scan images of the patient (Figure 24) and processing them in the 3D Slicer software (segmentation process). Figure 25 shows the resulting 3D model (STL file).

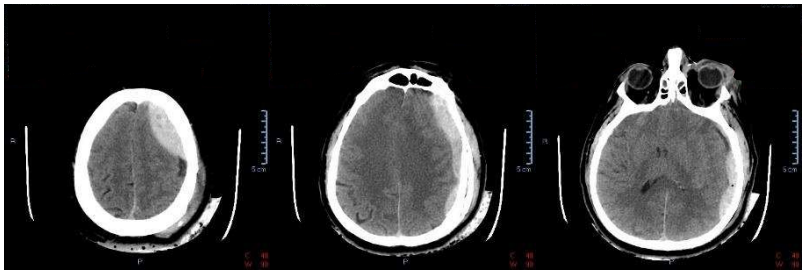

Figure 24. CT images of the patient. The DICOM files were used for the 3D reconstruction and segmentation of the skull. The hematoma is noticeable on the right side of the images (left side of the patient).

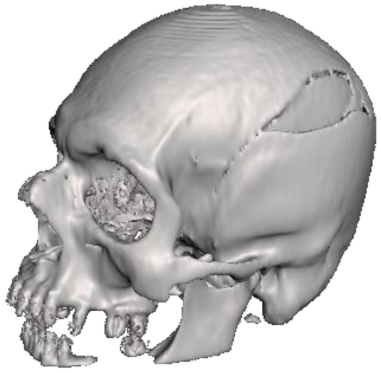

Figure 25. 3D model of the skull after segmentation of the CT images in 3D Slicer. The fracture is visible on the left side of the patient.

In order to reduce the cost and facilitate the fixation of the skulls for the practical training sessions, the skull was cut in the Meshmixer software to focus on the region of interest, thus removing the lower part of the model (Figure 26).

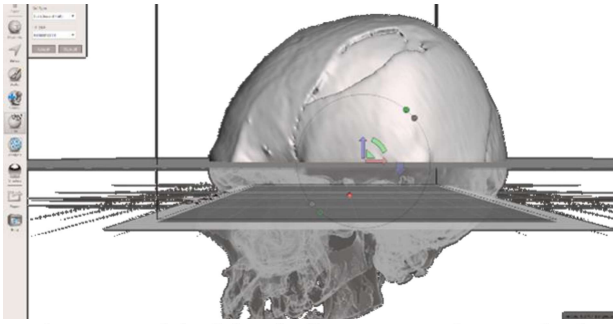

Figure 26. The 3D model of the skull was cut to keep only the region of interest for the training activity.

The resulting geometry was imported in SolidWorks software to define a completely flat plane on the bottom of the skull and to define the base (Figure 27), including four towers with internal holes for the fixation screws and an additional hole to fill the hematoma.

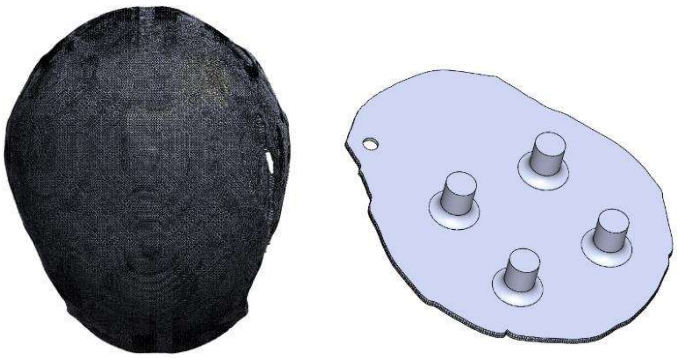

Figure 27. CAD modelling operations in SolidWorks to define the base with the fixation mechanism (right) starting from the segmented skull (left).

The base and skull were joined again in the Meshmixer software and laminated with Simplify3D to be 3D printed with PLA, just as a first trial. The printing was successfully completed, as shown in Figure 28.

Figure 28. 3D printed skull obtained in MEX technology with PLA filament.

After that, a new wall was added in the fracture zone to serve as container bag of the hematoma (Figure 29).

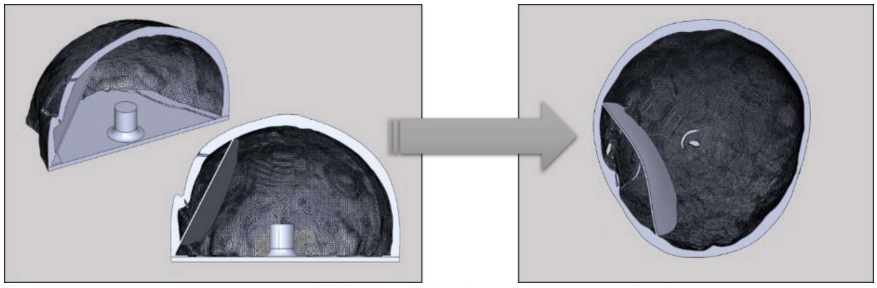

Figure 29. CAD modelling of the bag to retain the hematoma.

In parallel, a fixation mechanism was designed (Figure 30) to fix the skulls for the practical training sessions. The design consists of 4 parts that are joined by screws and with adjustable angle in one axis to the skull in the desired position.

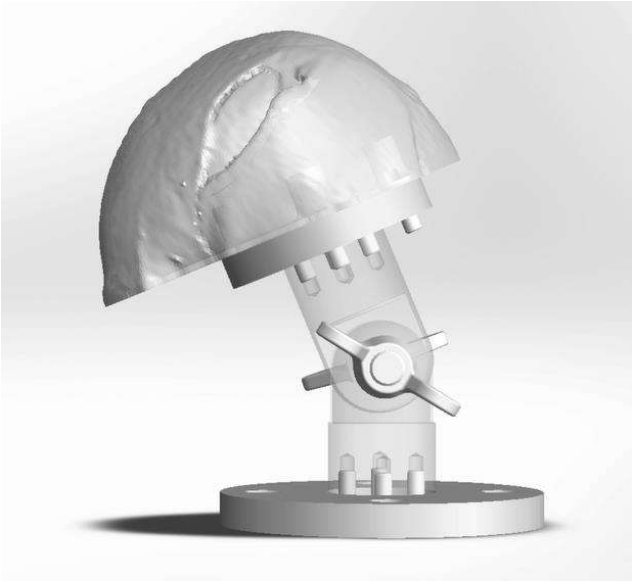

Figure 30. Design of the fixation mechanism of the skull, with adjustable angle and several possible positions of the skull.

The components of the fixation mechanism were machined (Figure 31) and a new skull with EP filament was produced (Figure 32).

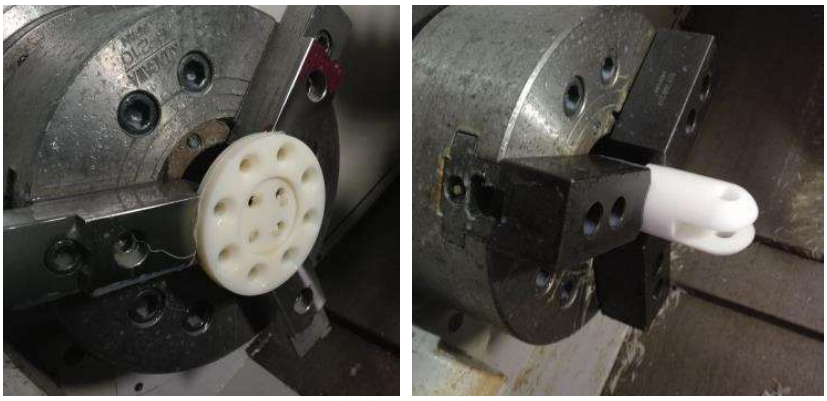

Figure 31. CNC machining (lathe) of the fixation system components.

Figure 32. 3D printed skull in MEX technology with EP filament.

The skull was screwed on the fixation system (Figure 33) and the assembly was used by the neurosurgeon to validate the geometry and material selected (Figure 34). Figure 35 shows the 3D printed skull after the validation test.

Figure 33. 3D printed skull with EP filament.

Figure 34. 3D printed skull during the validation test. The neurosurgeon gave a positive feedback of the material.

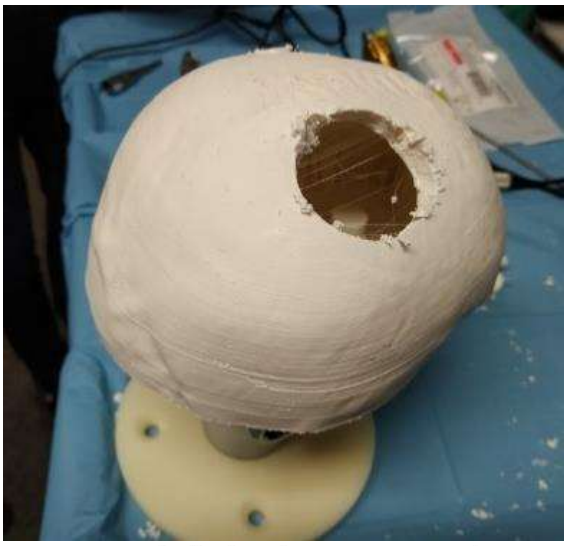

Figure 35. Skull after the neurosurgeon's test.

Although the neurosurgeon validated the material for the skull, one important detail was discussed regarding the geometry of the fracture. According to their knowledge, this fracture should have less joining points. As a consequence, the fracture was segmented again to reduce the contact area. Figure 36 shows the difference between the initial fracture and the final one.

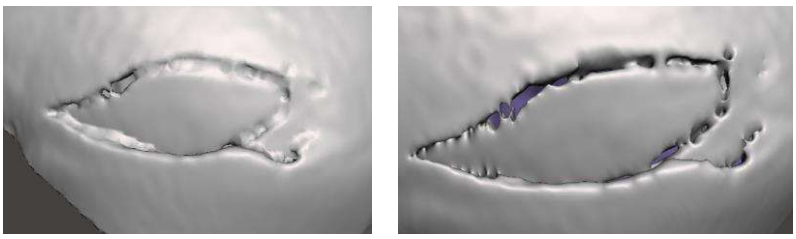

Figure 36. Modification of the fracture (left: original geometry of the fracture; right: new fracture).

Taking advantage of the new segmentation, the geometry of the hematoma bag was improved by defining a wall surrounding the hematoma, which was noticeable in the CT images (Figure 37).

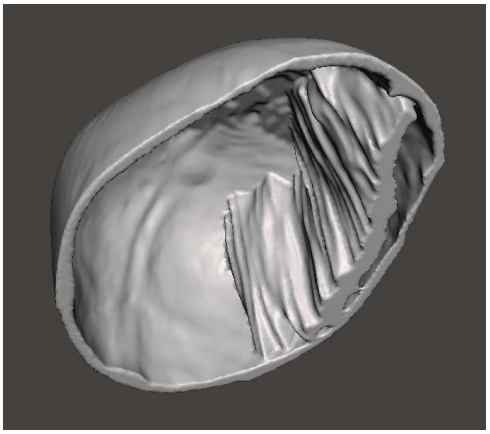

Figure 37. New hematoma bag.

The new model was 3D printed and it was observed that the hematoma cavity was not completely sealed. To solve this, the STL file after the segmentation was modified with different approaches. The first attempt consisted in adding spheres in Meshmixer all around the hematoma bag (Figure 38), but it did not work properly as in some cases the spheres were considered as removed material in the lamination software.

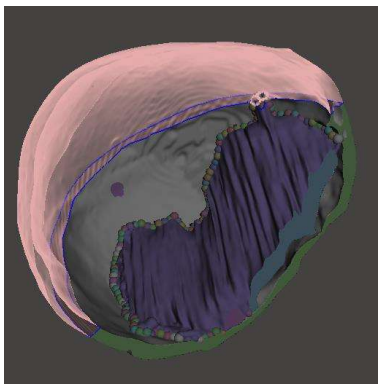

Figure 38. Hematoma bag with small spheres in the perimeter to try to seal the contour without success.

Finally, the sculpt feature in Meshmixer was the solution to seal the contour (Figure 39).

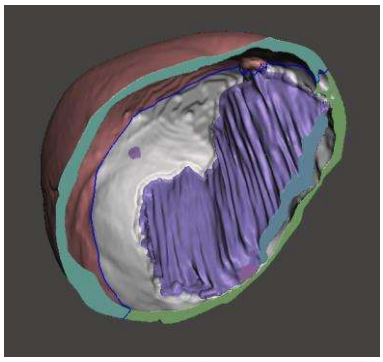

Figure 39. Hematoma bag with sealed contour (sculpt tool in Meshmixer).

With the final design of the fracture and hematoma bag, a 3D printed model was manufactured with EP to do a leakage test (Figure 40). Regarding the hematoma material, the solution of sodium alginate powder (from Acros Organics) with distilled water (1:20 w/w) was used (Figure 40). To properly fill the cavity of the hematoma, the fracture was sealed with Parafilm®.

Figure 40. Left: 3D printed model of the final geometry cover with Parafilm® for the leakage test. Right: Syringe with sodium alginate and distilled water (1:20 w/w) to mimic the hematoma.

The leakage test was successfully completed (no leaks in the cavity of the hematoma), although it was carried out in a skull without base. However, the base is needed to fix the skull to the fixation system and to seal the bottom of the hematoma cavity. Therefore, a hole was added in the base of the skull, properly located to be able to fill the hematoma cavity from the outside (Figure 41).

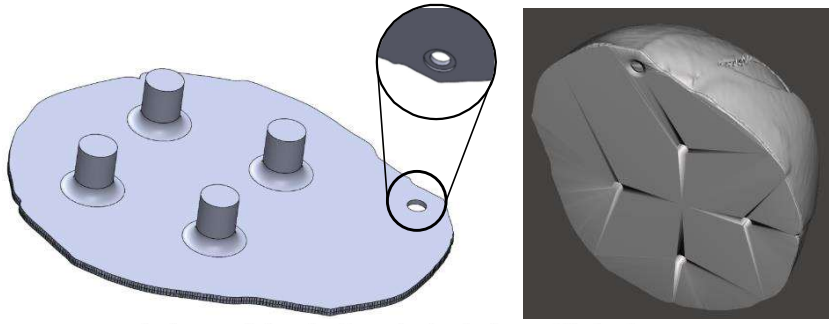

Figure 41. Left: base of the skull with the hole to fill the hematoma cavity. Right: final skull STL ready to 3Dprint, with the filling hole in the base.

The final design of the skull was laminated in Simplify3D software, using a printing temperature of 200 °C, layer height of 0.3 mm, extrusion width of 0.6 mm and infill density of 100%. The resulting

gcode file was run in an Atom 2.5 FX 3D printer, with an approximated printing time of 14 hours and 15 min. The result is depicted in Figure 42.

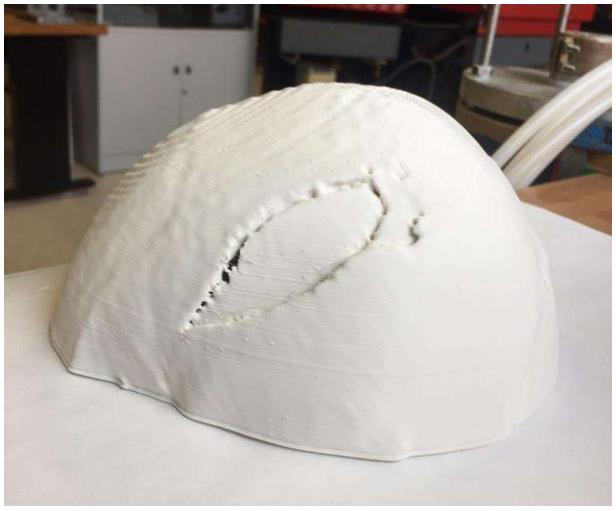

Figure 42. Final 3D printed skull of case 1 (intracranial hematoma with skull fracture).

Note that the 3D printing of the EP filament is more complex than in the case of PLA, especially for long prints. This is due to the higher brittleness of the EP filament (the teeth of the driver gear of the extrusion mechanism gradually remove small particles of the filament that lead to the blockage of the extrusion device). To avoid this, compressed air was applied in the extrusion mechanism to keep it clean (as the 3D printer uses a Bowden extrusion system, the hotend is far away from this air flow, which means that it does not affect the printing process).

The 3D printed skull was manually machined with a tap tool to make the internal thread of the four holes of the base. Then, the skull was placed and screwed in the fixation system. Figure 43 shows all the components previous to the assembly. Figure 44, Figure 45 and Figure 46 depict the assembly process.

Figure 43. 3D printed skull and components of the fixation mechanism before the assembly.

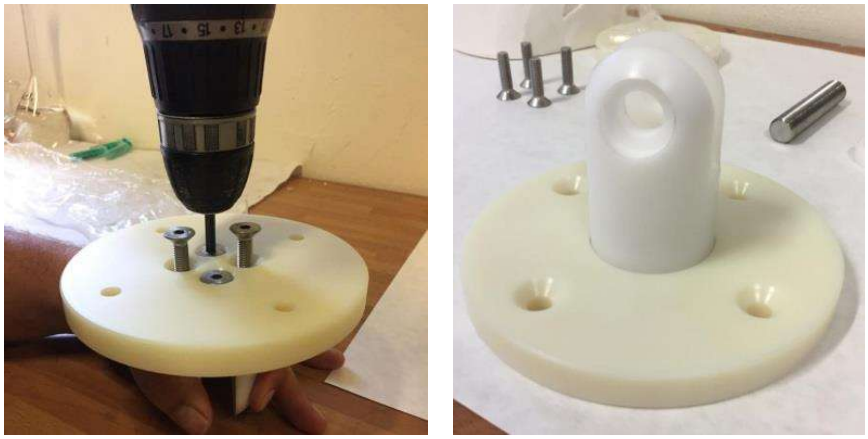

Figure 44. Assembly of the lower part of the fixation system.

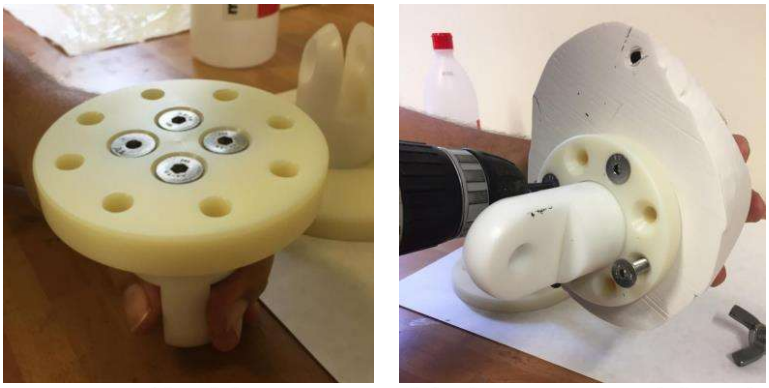

Figure 45. Assembly of the upper part of the fixation system (left) and skull (right).

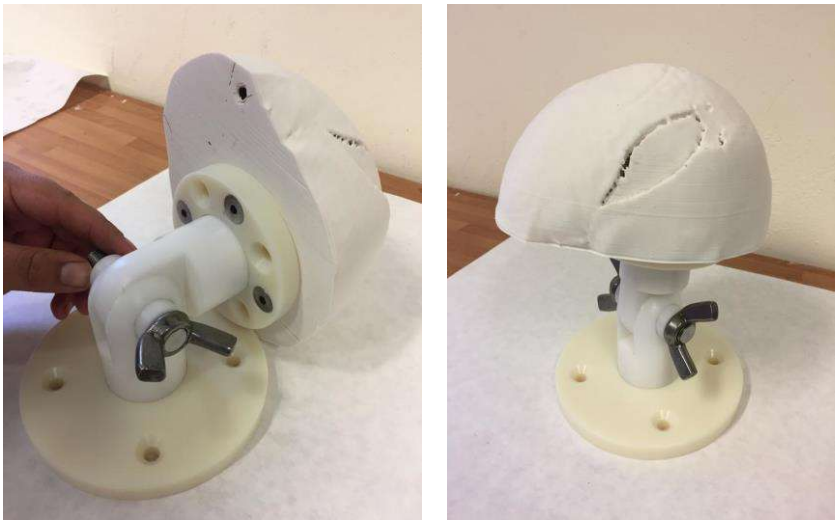

Figure 46. Skull assembled in the fixation system with adjustable angle.

Figure 47 shows the synthetic models prepared for the practical session with all the required tools for the surgery. Note that the sodium alginate solution was filled *in situ* just before the practical session and the hole was sealed with 3D printed cylindrical caps with flexible filament (Filaflex TPU).

Figure 47. Synthetic models of the intracranial hematoma with fracture prepared for the practical training (July 2019). The sodium alginate solution to simulate the hematoma was injected just before the practice in the hematoma cavity.

Figure 48 shows the developed skull being used during the training session.

Figure 48. Synthetic model during the practice.

1.1.2. Case 2: Intracranial hematoma (without skull fracture)

The second case consisted in another intracranial hematoma, but in this case the skull did not have any fracture. The process was similar to the previous one and the same materials were used (Smartfil® EP filament for the skull production in a material extrusion AM equipment and the solution of sodium alginate with distilled water at 1:20 w/w for the hematoma).

The process started with the segmentation of the real CT images (DICOM files). In this case, during the segmentation of the skull, a wall that surrounds the hematoma was also segmented to obtain the cavity of the hematoma (Figure 49). The complete segmented skull is depicted in Figure 50.

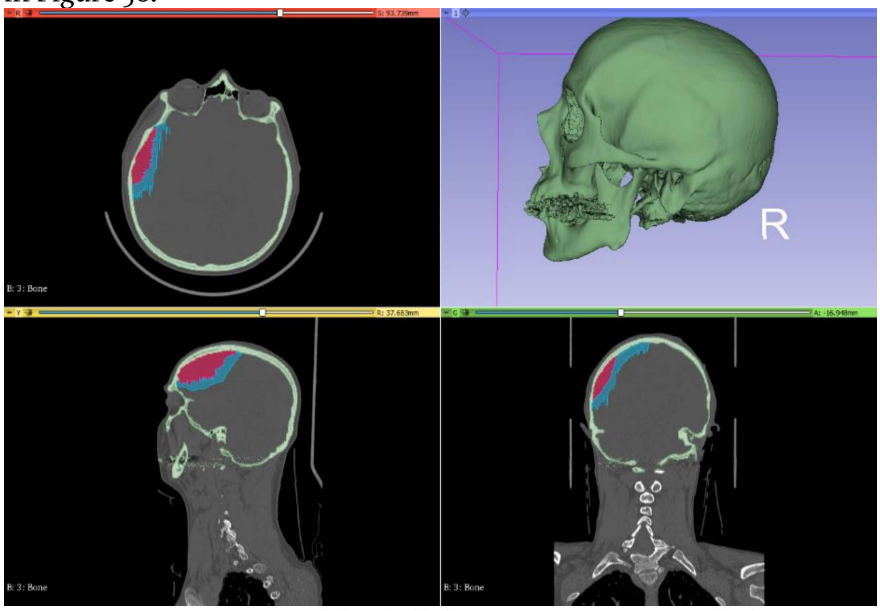

Figure 49. Segmentation of the skull from DICOM images. The hematoma is depicted in pink and the container wall of the hematoma in blue.

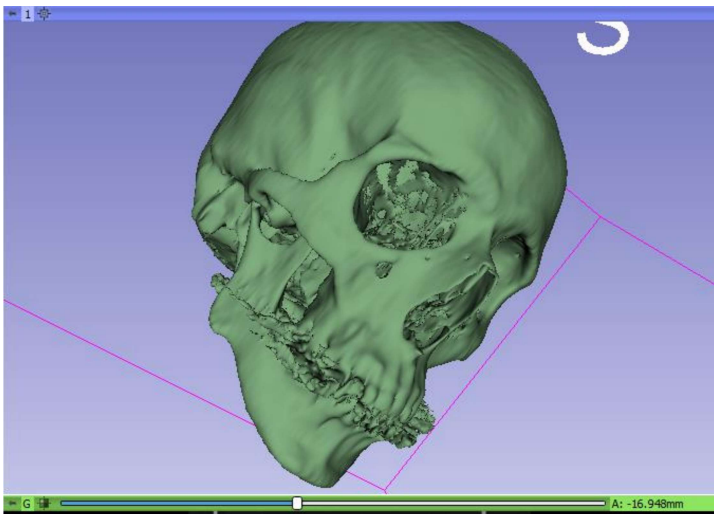

Figure 50. Reconstructed skull after segmentation.

The STL files of the skull and wall of the hematoma cavity were imported into Meshmixer and joined (combine feature). Afterwards, the lower part of the resulting skull was removed to simplify the model (the lower part was not needed for the practical training) (Figure 51).

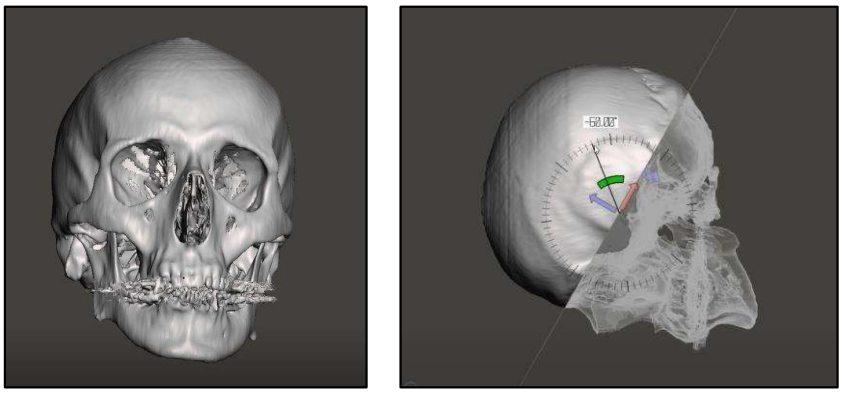

Figure 51. Cutting of the 3D skull in Meshmixer.

The resulting object was converted into solid STL and imported in SolidWorks (Figure 52).

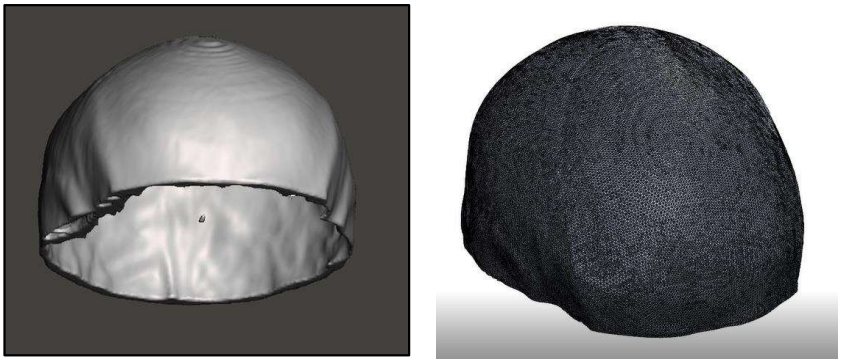

Figure 52. Cut skull in Meshmixer (left) and imported geometry in SolidWorks (right).

As the plane cut feature in Meshmixer leaves a non-planar surface, an additional cutting was carried out in SolidWorks. After this, an extrusion feature was applied to create the base of the skull (Figure 53). Apart from this, the towers and holes for the fixation screws were added (Figure 54).

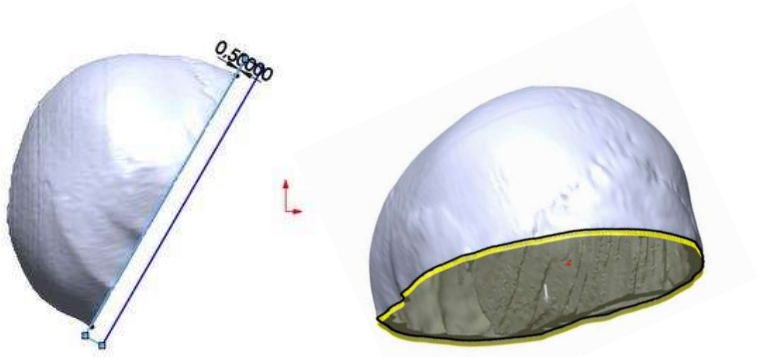

Figure 53. Cutting and extrusion features in SolidWorks to define the base of the skull.

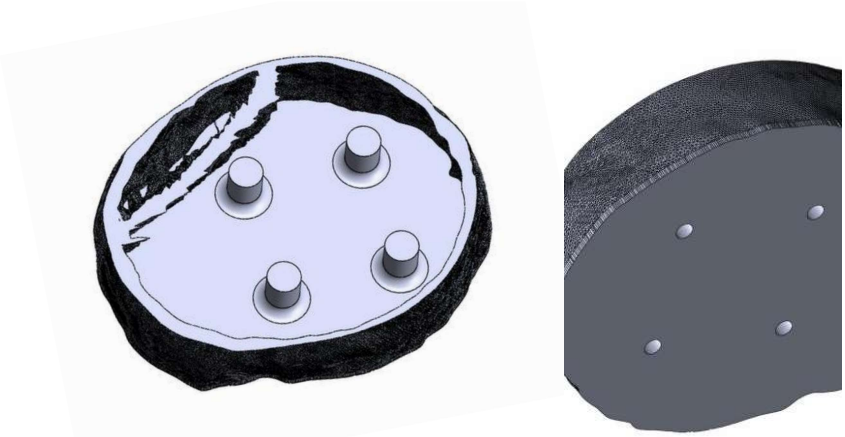

Figure 54. Towers (left) and holes (right) to fix the skull to the fixation mechanism with screws.

In this case, as the hematoma cavity did not have enough space on the base, an additional channel was added to connect the cavity with outside, so that the simulated hematoma material (solution of sodium alginate) could be injected (Figure 55). Figure 56 shows the final design of the skull, including the base and filling channel.

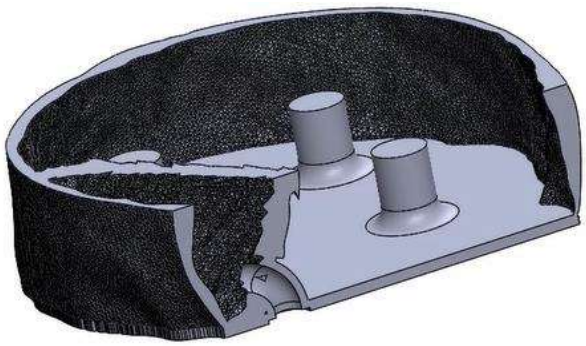

Figure 55. Section view of the 3D skull geometry with additional channel connecting the outside with the hematoma cavity to inject the sodium alginate solution.

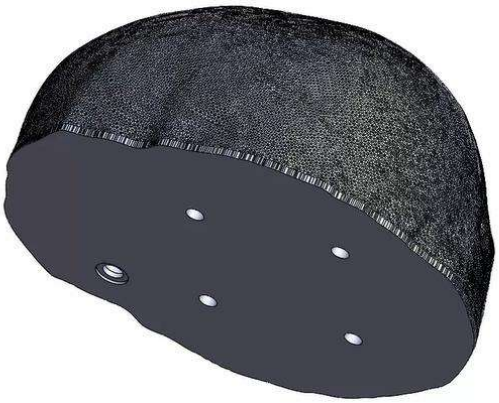

Figure 56. Final design of the skull.

The STL file of the final design was imported in Simplify3D and laminated with the same printing parameters as case 1. Figure 57 and Figure 58 show some screenshots of this step.

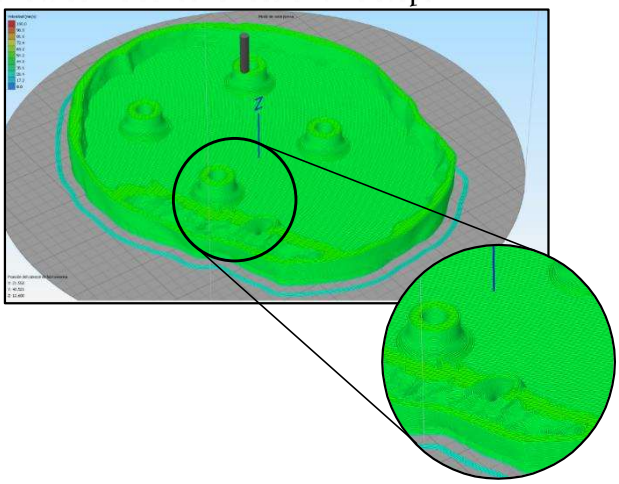

Figure 57. Lamination of the base in Simplify3D, with detail of the filling channel.

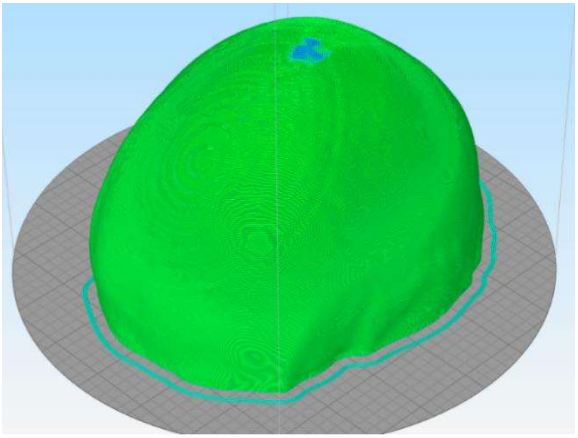

Figure 58. Complete view of the model in Simplify3D software.

The resulting manufacturing file (gcode file) was run in the 3D printer (Atom 2.5 FX) and the skull was obtained after several hours of 3D printing (Figure 59).

Figure 59. Final 3D printed skull.

Figure 60 shows the skull already assembled in the fixation mechanism.

Figure 60. 3D printed skull assembled in the fixation system.

Figure 61 shows the skull during the practical training of students (after the cutting of bone, removal of the hematoma and suture of the removed bone). Note that the sodium alginate solution to emulate the hematoma was also filled *in situ* before the practical session (the hole of the base was sealed with the cylindrical and flexible 3D printed caps, as in case 1).

Figure 61. Synthetic model of case 2 during the practical training.

1.2. Training material for surgery of brain tumor

The second summer school of the BrainIT project (initially scheduled for July 2020, but delayed due to the pandemic situation) focused on neuro-oncology. For the practical sessions, two real cases of brain tumor have been developed:

- Meningioma case, which is a brain tumor arising from the meninges (the membranous layers surrounding the brain). The consistency of the tumor is higher than the one of the brain.
- Glioma case, which is a brain tumor located in any area of the brain and with lower consistency than the brain (removable by vacuum).

As in the previous section, both cases had to be developed starting from the DICOM images of the patients and with low-cost manufacturing approaches (material extrusion AM). Ten replicas of each case had to be obtained for the practical training sessions. In both cases, the students will cut the skull and access the tumor to be removed with hand tools (meningioma) or by vacuum (glioma). Finally, the removed bone will be sutured again.

The first activity to develop these cases focused on the selection of the manufacturing process and materials.

For the production of the skulls, the same approach of the previous cases was used (material extrusion AM of Smartfil® EP filament). However, since the printability of this filament is less reliable than standard PLA, the skulls were divided in two zones: the working area, where the students will cut and suture; and the rest of skull. The idea was to use Smartfil® EP filament for the working area and PLA for the rest. This way, the risk of blockage of the extrusion driver of the 3D printer would be drastically reduced, thus improving the reliability of the printing and, at the same time, keeping the quality of the synthetic models as the PLA filament would only be used in the non-working areas. Moreover, in order to facilitate the cutting process of the skull, which will be carried out with a Gigli saw, it was proposed to reduce the infill density of the printing process to avoid the blockage of the tool. To properly select the best infill density, several plates with different infill densities (10, 20, 30, 50, 75 and 100%) were 3D printed and cut with saw to qualitatively analyze the behavior (Figure 62). Therefore, the

infill density for the working area was 30%, while the rest of the skull (PLA filament) would be printed with 20% of infill density.

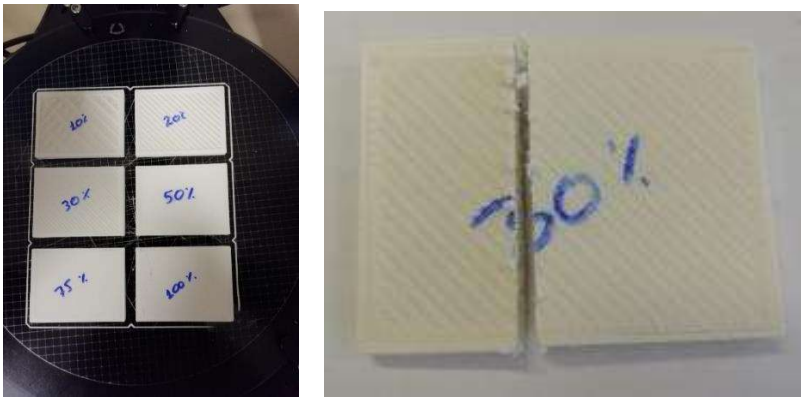

Figure 62. Samples with different infill densities (10, 20, 30, 50, 75 and 100%) to be cut with saw (left) and sample with the selected infill density after the cutting (right).

For the manufacturing of the brain, the approach consisted in using different liquid thermoset materials poured and polymerized in a 3D printed mold (also manufactured with material extrusion AM) to reproduce the desired geometry. Three different materials were analyzed in the preliminary tests:

- AljaSafe®: alginate used to produce molds. This material was processed in different concentrations but it was discarded due to its dimensional instability and higher stiffness compared to the real brain.
- Contor 5005: three-component silicone (A, B, C) with tin catalyst. Six cylindrical samples of five different proportions (30 samples in total) were manufactured with this material. The A:B ratio was maintained according to the manufacturer's recommendation (100:2.5) while the C content compared to A+B was modified (30, 50, 70, 90 and 100% of C component). The codes used for the five different groups were C30, C50, C70, C90 and C100.
- Ecoflex® 00-10: two-component silicone (A, B) with platinum catalyst (B). Six cylindrical samples of three different proportions were

manufactured with this silicone. The A:B ratios were 1:0.5 (codified as E0.5), 1:1 (E1) and 1:1.5 (E1.5).

Figure 63 shows samples of both silicones. These samples were subjected to compression tests with 10 mm/min of crosshead speed (Figure 64) and weighed every day for approximately one month to check their dimensional stability (no significant variations were observed).

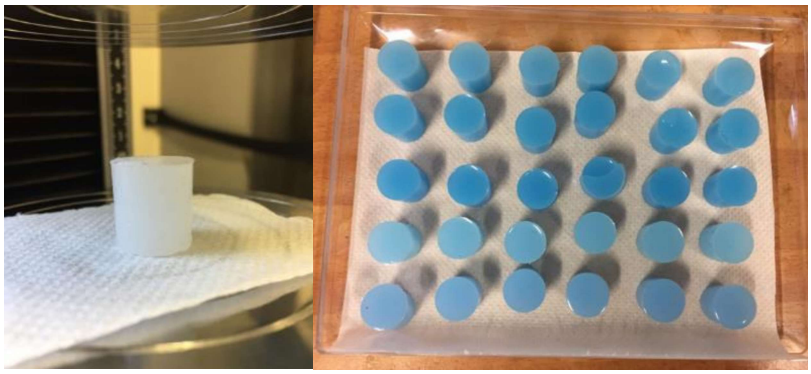

Figure 63. Sample of Contor silicone (left) and samples of Ecoflex® 00-10 (right) before the compression tests.

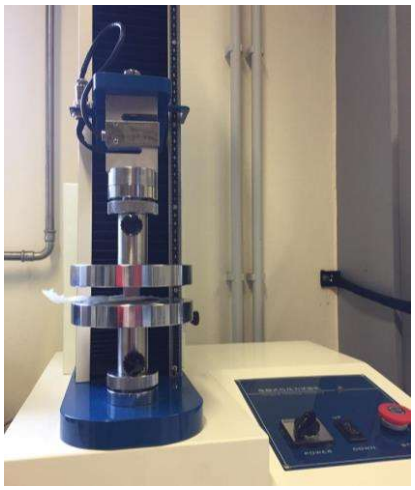

Figure 64. Sample during compression test.

The results (average value and standard deviation) of the compression tests are shown in Figure 65. According to the literature,

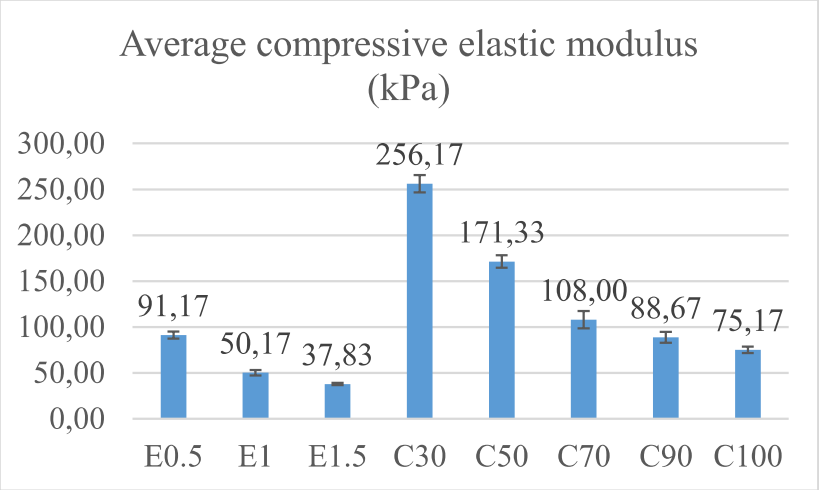

Figure 65. Compressive elastic modulus (average and error bars according to the standard deviation) of the different groups tested (Contor 5005 and Ecoflex® 00-10 silicones).

Table 5. Reference values of brain elastic modulus.

Brain elastic modulus (kPa)	**Reference**
71.7 (*Dynamic modulus value*)	[5]
5.96 (gray matter) **2.68** (white matter)	[6]
490.3 (gray matter) **49** (white matter)	[7]
10 (gray matter) **10** (white matter)	[8]
2.1 – 2.7 (gray matter) **2.1 – 6** (white matter)	[9]
3.24	[10]
73 (gray matter) **32** (white matter)	[11]
3.15	[12]

From the previous data, the average value was estimated, but considering the highest value an outlier. The obtained average value (21.16 kPa) was lower than the value of the tested silicones. In any case, one sample of each group was produced again (Figure 66) to be directly tested by an experienced neurosurgeon.

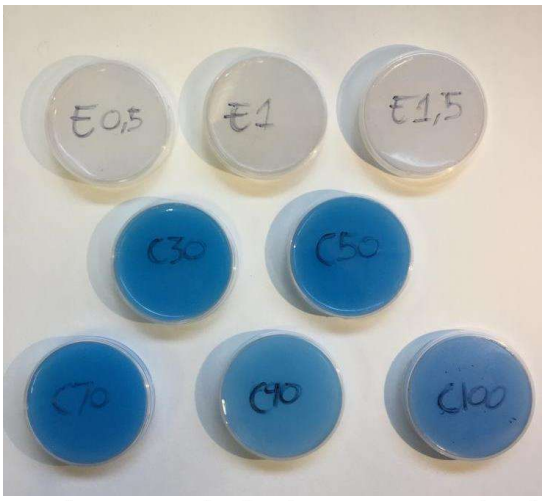

Figure 66. Silicone samples for the neurosurgeon's validation.

Among them, the preferred one was E1.5, which was the one with the lowest elastic modulus. However, other tests carried out by the neurosurgeons participating in this project recommended an even lower stiffness to improve the similarity to real brain tissue. For this to happen, a new component was included, following the recommendation of the manufacturer of this silicone. This new component, called Slacker, reduces the stiffness of the molded silicone. In order to find the best proportion, 4 different groups with different proportions of the silicone components and slacker (A:B:Slacker) were produced (Figure 67 ,six replicas of each group) and subjected to compression tests. The results are shown in Table 6.

Figure 67. Final silicone samples for the compression tests.

Table 6. Average compressive elastic modulus for the four silicone groups tested.

Groups of samples (A:B:Slacker)	**Average elastic modulus (kPa)**
Group 1 (1:1:1)	40.41
Group 2 (1:1:2)	37.90
Group 3 (1:1:3)	31.29
Group 4 (1:1:4)	27.95

As expected, the slacker allowed the reduction of the elastic modulus of the samples. Among the produced samples and in accordance with the neurosurgeons' feelings, the best material to mimic the brain was group 3 (1:1:3), which had an elastic modulus of 31.29 kPa. Therefore, this mixture was selected as the optimal one for the brain. However, the Slacker component is considerably more expensive than

the other ones. For this reason and with the objective of keeping a low-cost approach, the brain of the two cases was divided into 2 different zones: the working area (zones affected during the training session), which was manufactured with 1:1:3 ratios (A:B:Slacker) of Ecoflex® 00-10; and the non-working area (the rest of the brain that will not be used by students during the surgery training), which was produced with the 1:1 ratio (A:B, without Slacker).

On the other hand, note that between the brain and the skull there are 3 membranes. In this case, the most important layer (the dura mater) will be reproduced. Dura mater is a membrane with a greater consistency than brain. For this reason, the mixture chosen to reproduce this tissue was Ecoflex 00-10 with 1:1 ratio (A:B). The dura mater was produced by pouring this mixture on a flat surface and laminating the blend with a roller to obtain a thin sheet that will be located between the skull and the brain during the assembly.

Regarding the molds and insert tools needed for the silicone molding of the different components (such as the brains and the tumor of case 1), material extrusion AM with PLA filament were used (with 20% of infill density). The PLA filament was chosen due to its stability and speed for 3D printing.

1.2.1. Case 1: Meningioma.

This type of tumor has a higher consistency than brain. For this reason, a stiffer blend compared to the brain was used to produce the tumor (1:1 rate of components A:B of Ecoflex 00-10). Furthermore, considering that this tumor is reddish in color and contains calcium deposits, it was decided to add a small amount of a red pigment (3% of the total mass), in addition to crushed PLA that simulates calcification, thus achieving a more realistic model.

Once selected the materials for the different components, the 3D reconstruction was made by using the CT scan of the patient and processing them in the 3D Slicer software (segmentation process).

First of all, the skull was segmented (Figure 68) and cut to obtain the final model (Figure 69).

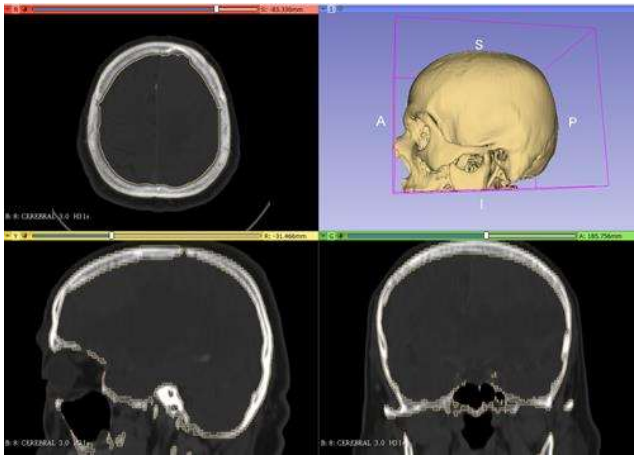

Figure 68. Segmentation of the skull from the DICOM images.

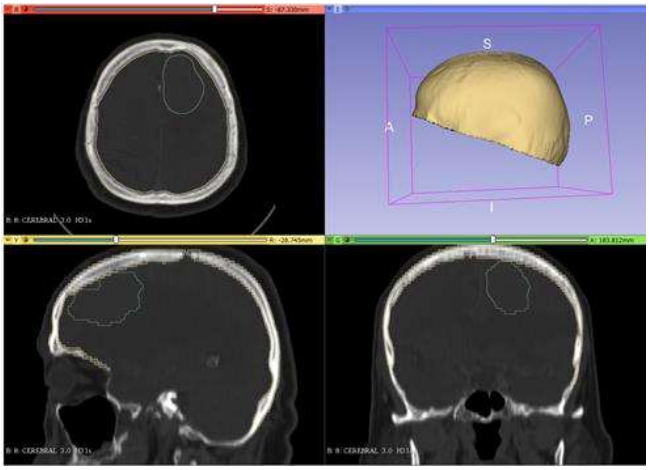

Figure 69. Cutting of the 3D skull in 3DSlicer.

As previously mentioned, the tumor mold is required to be able to pour the silicone mixture later. Therefore, once the tumor was segmented (Figure 70), a copy of this model was made with an added thickness of 10 mm. The original segment was subtracted, generating the mold of this model (Figure 71).

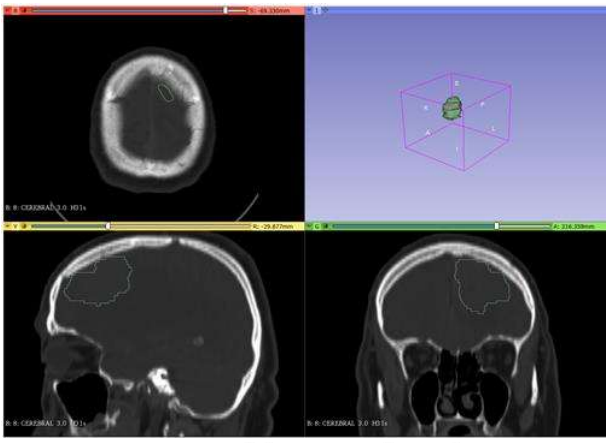

Figure 70. Segmentation of the tumor from the DICOM images.

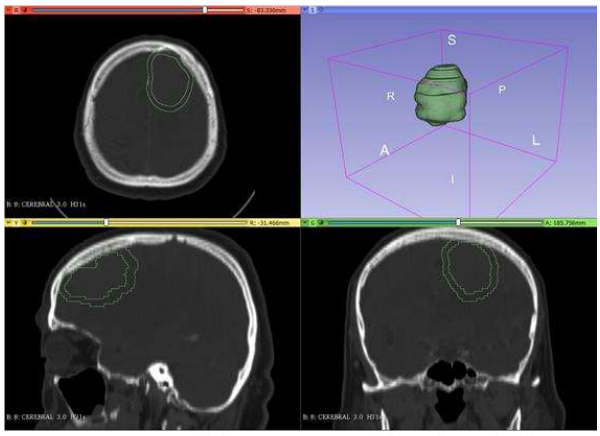

Figure 71. Segmentation of the tumor mold with a thickness of 10 mm.

To create the brain mold, the model in Figure 68 (skull) and the model in Figure 70 (tumor) were joined so that the molded brain could have the void to assemble the tumor. Moreover, the thickness of the resulting geometry was increased 3 mm so that the molded brain had 3 mm clearance with the skull (Figure 72). The resulting geometry was cut to remove the lower part of the model (Figure 73).

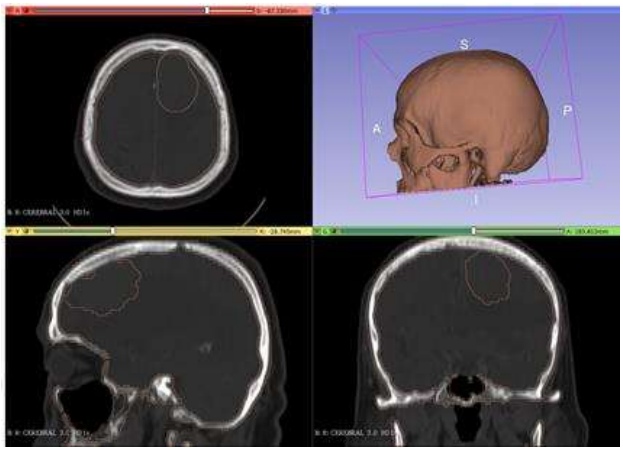

Figure 72. Segmentation of the brain from the DICOM images.

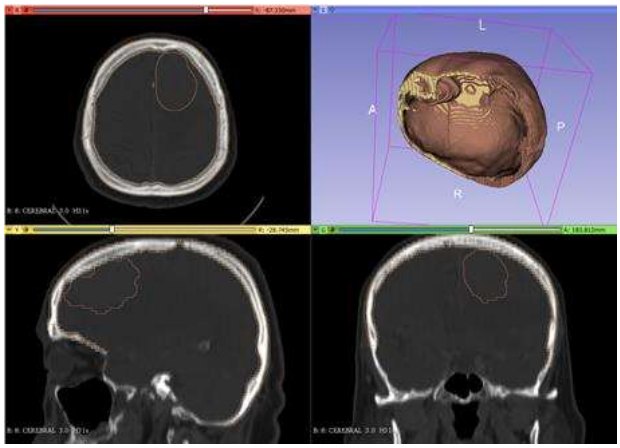

Figure 73. Brain mold obtained from the DICOM images after cutting the lower part.

Once these models were segmented, the STL files of the skull, tumor mold and brain mold were imported into Meshmixer, where all of them were converted into solid STL (Figure 74) and imported in SolidWorks.

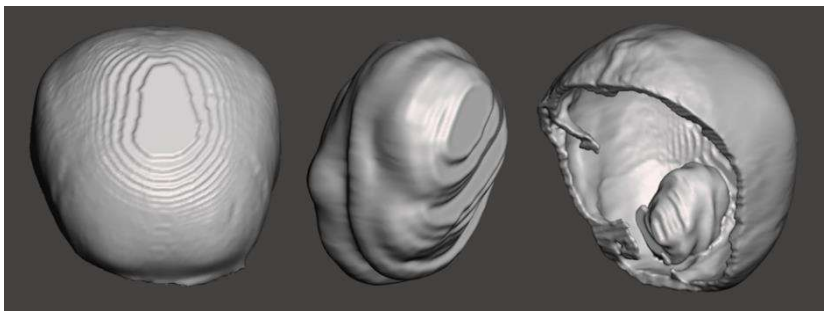

Figure 74. Models of case 1 in Meshmixer.

Regarding the skull model, the first feature carried out was a cutting operation with a well-referenced flat plane to obtain a perfectly flat surface on the bottom of the skull. Afterwards, some tabs were added to be able to assemble this part of the skull with the base (Figure 75). Note that the base of the scale is an independent part that allows assembling the dura mater, brain and tumor inside the skull and then screwing the base to fix all the components to the fixation system (Figure 30).

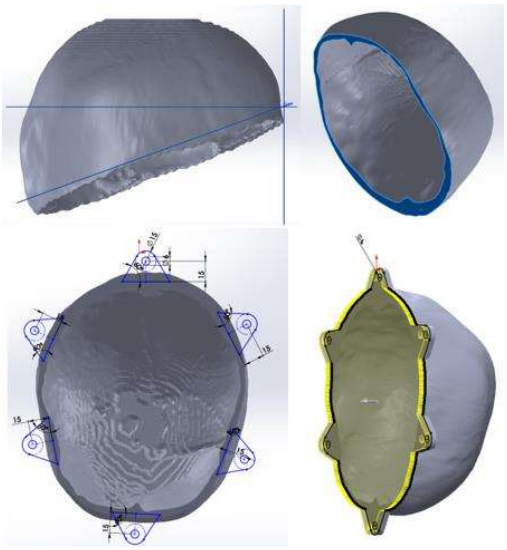

Figure 75. Initial features performed with SolidWorks for the skull design.

Afterwards, the working area was defined (Figure 76) to divide the skull into 2 parts. This way, the working area will be 3D printed with the selected EP filament and 30% infill density, and the rest with PLA filament and 20% infill density. Moreover, the tabs to screw the base of the skull were modified and placed inside the mold for aesthetics (Figure 77).

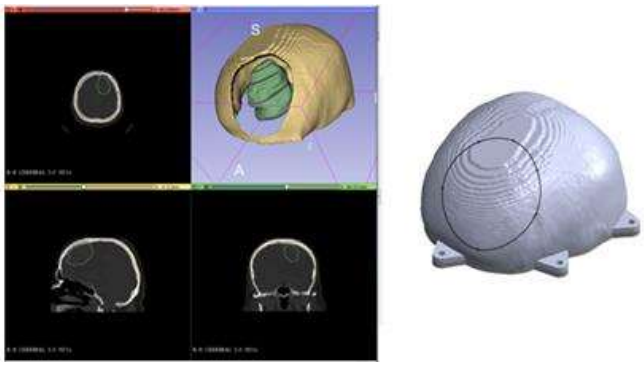

Figure 76. Image of the segmentation with a cut in the skull in the location of the tumor (left) and definition of the working area of the skull (right) to change the material during 3D printing (EP for the working area and PLA for the rest of the skull).

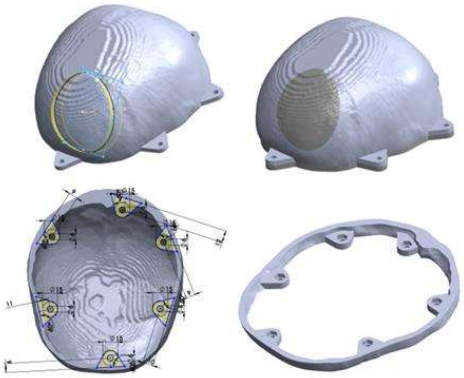

Figure 77. Features performed with SolidWorks to divide the model into the working and non-working areas (top) and modification of the housings for the assembly (hidden housing).

The base of the skull was also defined according to the screw tabs of the upper part of the skull (Figure 77). Moreover, the holes to fix the base to the fixation mechanism (holder) were also defined according to holder design (Figure 78).

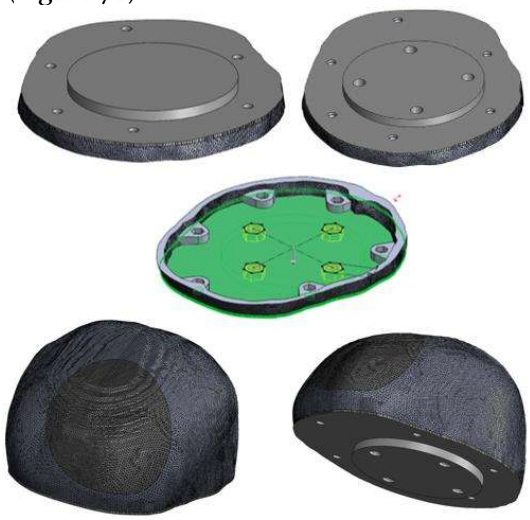

Figure 78. Features performed in SolidWorks for the skull base design.

The resulting manufacturing file (gcode file) was run in the 3D printer (Atom 2.5 FX) and the skull (Figure 79) and the skull base (Figure 80) was obtained after several hours of 3D printing.

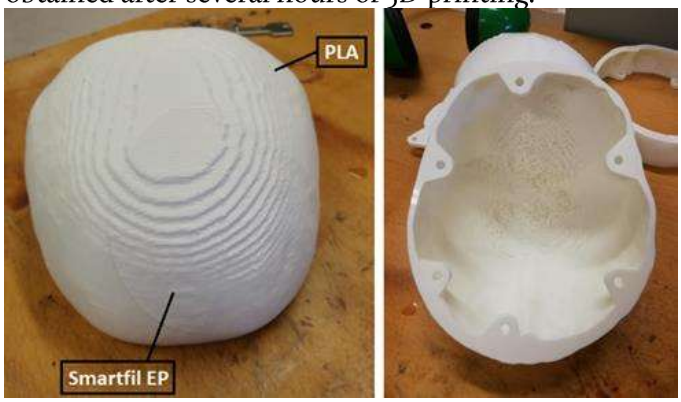

Figure 79. Final 3D printed skull.

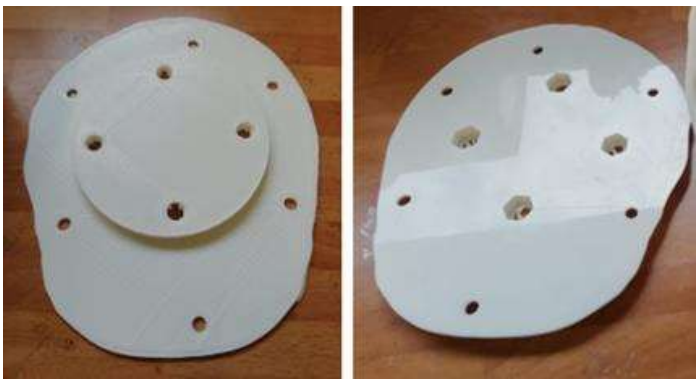

Figure 80. Final 3D printed skull base.

Regarding the brain mold model, the segmented mold (Figure 74) was cut to define a flat plane and then, divided into two parts to facilitate the demolding process, especially in the region of the tumor (Figure 81).

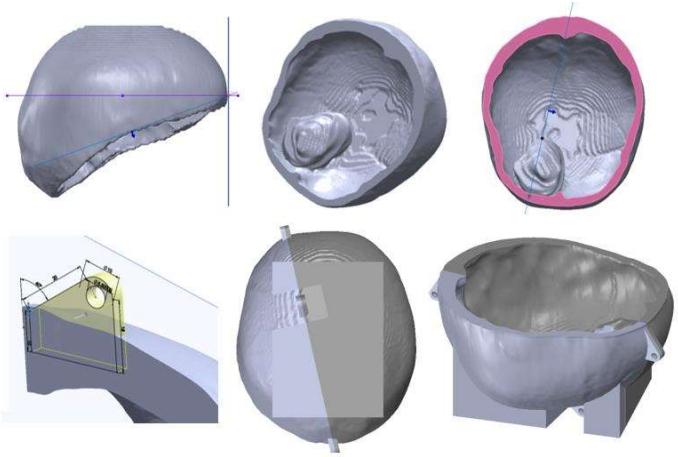

Figure 81. Design steps in SolidWorks to obtain the final geometry of the brain mold.

The result of the 3D manufacturing process of the brain mold is shown in Figure 82.

Figure 82. Final 3D printed brain mold.

Regarding the tumor mold, several features were applied to divide the initial geometry into two parts for the demolding process. Additionally, some tabs were added to join both parts of the mold and a feeding hopper to pour the silicone (Figure 83). Figure 84 shows the 3D printed tumor mold.

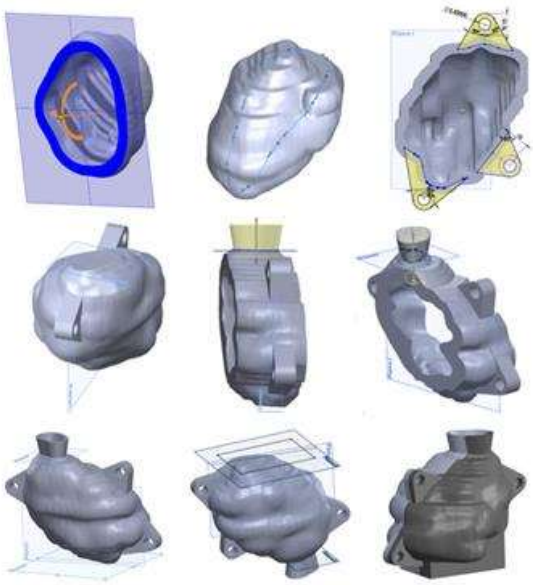

Figure 83. Design steps in SolidWorks to obtain the final geometry of the tumor mold.

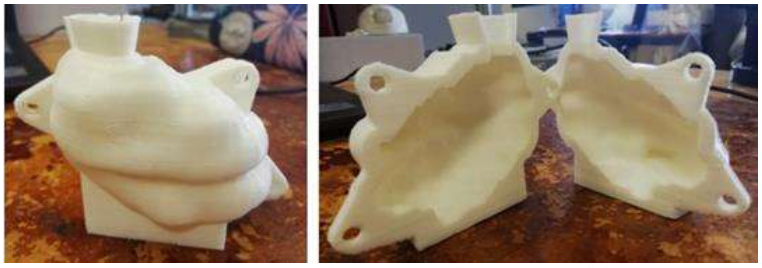

Figure 84. Final 3D printed tumor mold.

As mentioned before, the brain will be produced with two different mixtures of silicone: the softest selected mixture for the working area, and the hardest mixture for the rest of the brain. Therefore, two different pouring processes must be carried out. Figure 85 shows the design steps of the mold to define the working area. This mold surrounds the tumor, leaving a certain clearance between the tumor and the mold so that the softest silicone can cover the tumor, which is

already defined in the mold of the brain. The mold of the working area also has a ring that perfectly fits with the upper part of the brain mold to correctly place it before pouring the silicone.

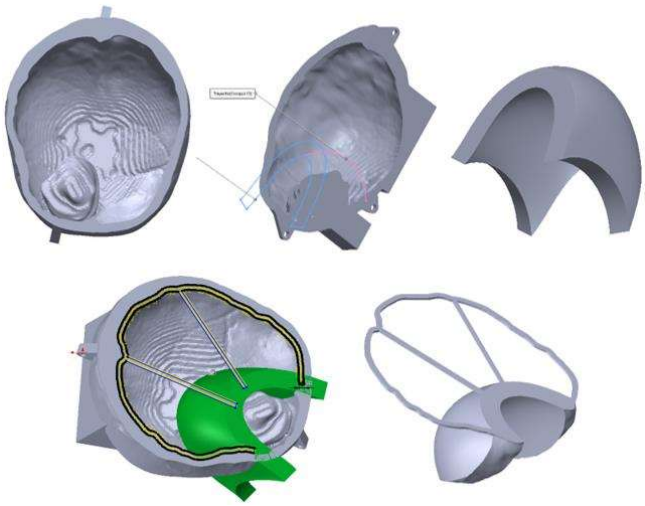

Figure 85. Design steps in SolidWorks to obtain the mold to define the working area.

Figure 86 shows the 3D printed mold of the working area and the final assembly with the brain mold.

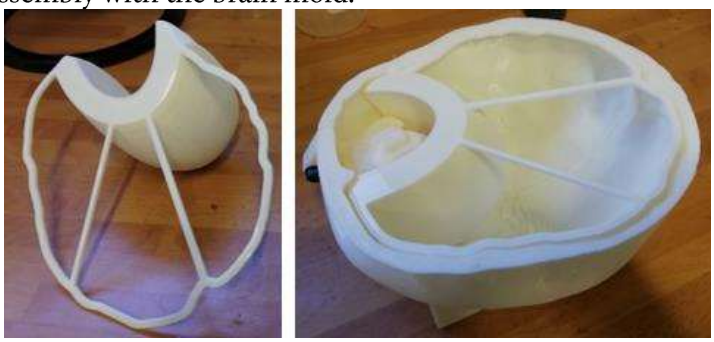

Figure 86. Final 3D printed mold of the working area (left) and assembly with the brain mold (right).

Once all the 3D printed models were obtained, the silicone mixtures that were necessary to make the brain (with the two different mixtures: the working area and the non-working area), the tumor and the dura mater were produced.

To make the brain, the mold to define the working area was placed inside the brain mold and the first pouring was made inside this mold with the chosen mixture of 1:1:3 (Ecoflex 00-10 component A:B:Slacker) (Figure 87). Then the rest of the mix without the Slacker was poured into the brain mold (Figure 88).

Figure 87. 1:1:3 silicone mixture inside the mold that defines the working area (left) and cured mixture (right).

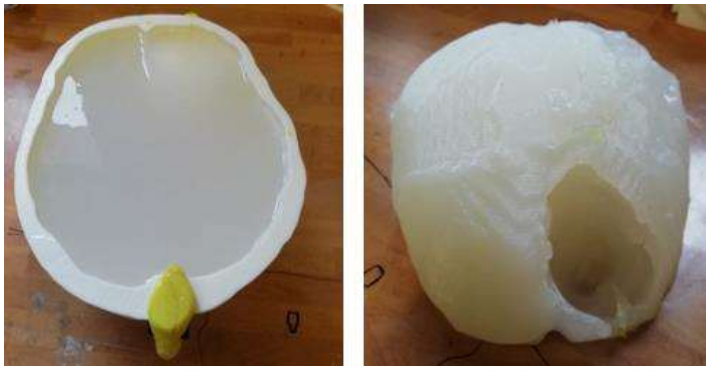

Figure 88. Pouring of 1:1 silicone mixture into the brain mold (left) and final brain model (right).

For the tumor, the 1:1 silicone mixture with pigments and crushed PLA was poured into the tumor mold (Figure 89). Figure 90 shows the final tumor model.

Figure 89. Mixture made for the preparation of the tumor (left) and mold filling (right).

Figure 90. Final tumor model.

Finally, to simulate the dura mater, 1:1 silicone mixture was expanded on a surface, after applying a previous layer of release agent, and left as thin as possible to make a thin sheet (Figure 91).

Figure 91. Thin sheet made with 1:1 silicone mixture to simulate the dura mater.

To finish case 1, the assembly of the full-scale models was carried out, as shown in Figure 92 and Figure 93, and the model was placed in the fixation mechanism (Figure 94).

Figure 92. Skull (left) and brain model with the meningioma inside (right).

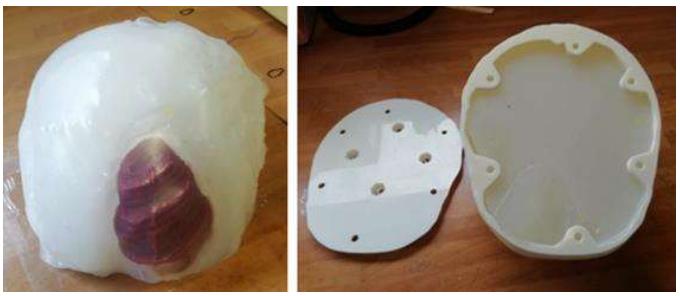

Figure 93. Incorporation of the dura mater layer on the brain model (left) and introduction of the brain into the skull (right).

Figure 94. Final model of case 1 on the stand.

1.2.2. Case 2: Glioma

This tumor has a lower consistency than brain. For this reason and with the experience obtained with the material chosen to emulate the hematoma of case 1 of the first summer school (Figure 40), it was decided to simulate this model with a mixture of sodium alginate with distilled water in a ratio of 1:20 w/w.

The process started with the segmentation of the real CT images (DICOM files). In this case, the models to be segmented will be the same as in the previous case, except the tumor, which will not be poured in a

mold, but inside the molded brain. Therefore, a cavity must be defined inside the molded brain to pour the sodium alginate solution that mimics the tumor.

The first model to be segmented was the skull (Figure 95). Also, as in Figure 69, the lower part of the skull was cut out (Figure 96).

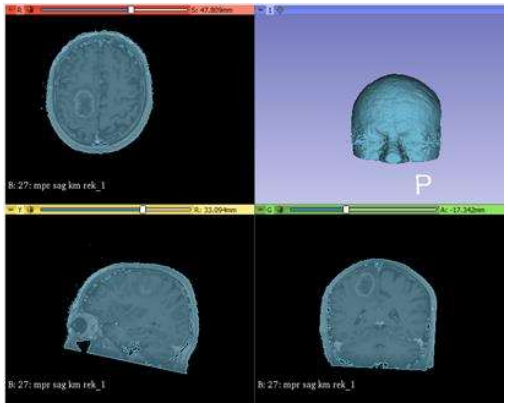

Figure 95. Segmentation of the skull from the DICOM images.

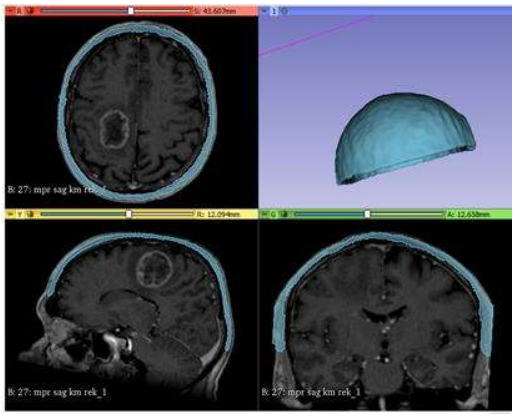

Figure 96. Cutting of the 3D skull in 3DSlicer.

To create the brain mold, the brain was first segmented by the succession of CT layers (Figure 97). Next, the thickness of this model was increased 10 millimeters and finally, the original brain model was

removed, thus leaving the interior empty and creating the mold (Figure 98).

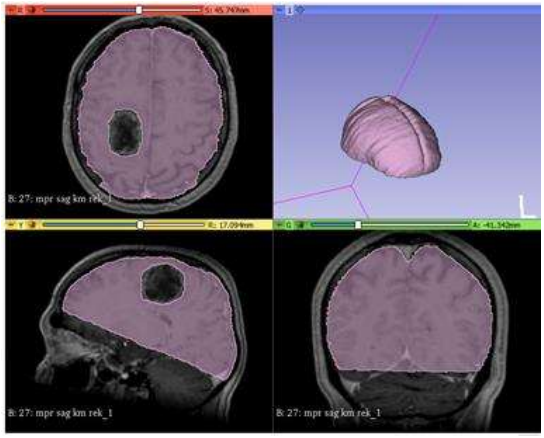

Figure 97. Segmentation of the brain from the DICOM images.

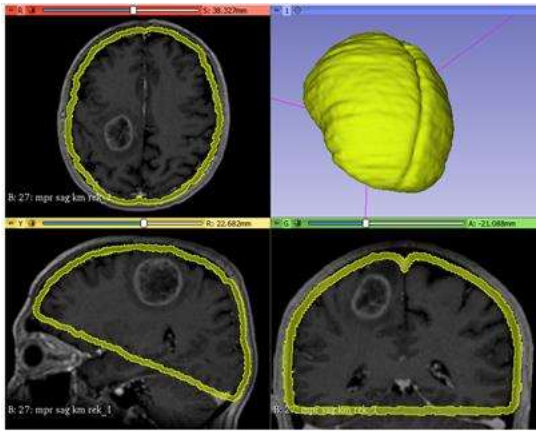

Figure 98. Segmentation of the brain mold with a thickness of 10 mm.

As in the previous models (Figure 95 and Figure 97), the tumor was segmented by the different CT layers, creating the tumor model shown in Figure 99.

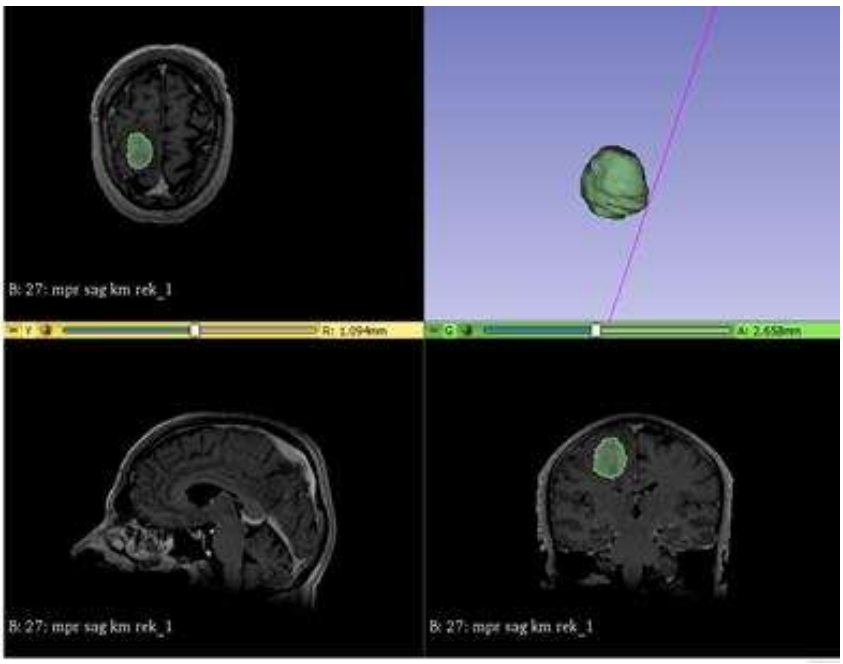

Figure 99. Segmentation of the tumor from the DICOM images.

Once the segmentation process was finished, the models were imported in STL files into Meshmixer and converted into solid STL (Figure 100).

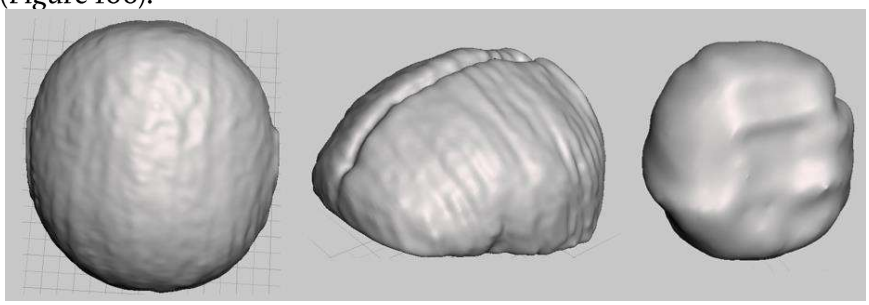

Figure 100. Models of case 1 in Meshmixer.

For the final definition of the skull, a flat cutting and the definition of the assembly tabs of the skull were designed (Figure 101).

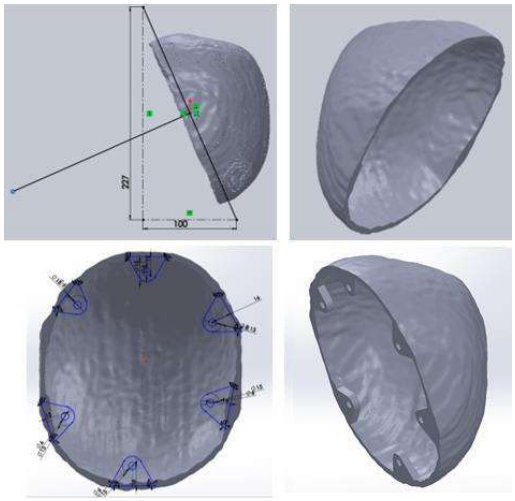

Figure 101. Initial features performed with SolidWorks for the skull design.

For the skull base, the same steps as in case 1 were followed (Figure 102).

Figure 102. Features performed in SolidWorks for the skull base design.

The skull was divided into two zones: the working zone (with EP filament and 30 % infill density), and the rest (PLA filament with 20% infill density). Figure 103 shows these steps.

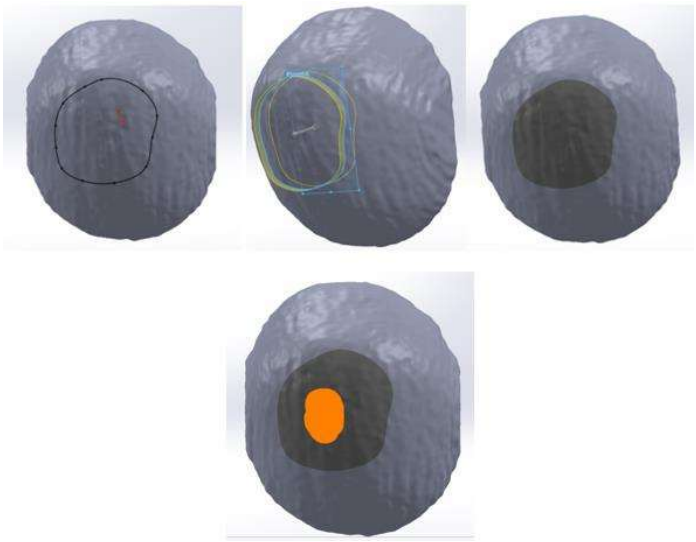

Figure 103. Features performed with SolidWorks to divide the model into the working and non-working areas (top) and image of the location of the tumor to ensure that correct the definition of the working area (bottom).

The result of the skull and the base skull model is depicted in Figure 104.

Figure 104. Final 3D printed skull.

For the brain mold, unlike the brain mold of case 1 (Figure 81), it was not necessary to divide it into two parts. Figure 105 shows the design steps (flat cut and definition of the base for stability during the silicone pouring).

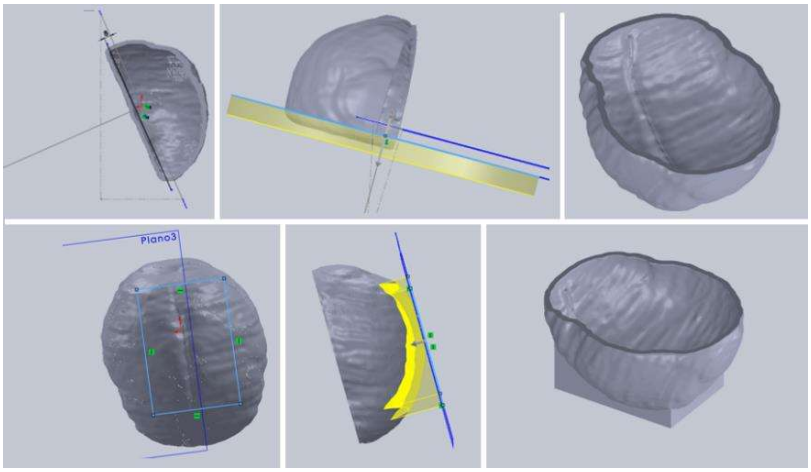

Figure 105. Design steps in SolidWorks to obtain the final geometry of the brain mold.

Figure 106 shows the 3D printed brain mold.

Figure 106. Final 3D printed brain mold.

For the design of the mold that defines the working area, a part was modeled covering the tumor with a certain clearance and adding a hopper to pour the silicone inside this mold (Figure 107).

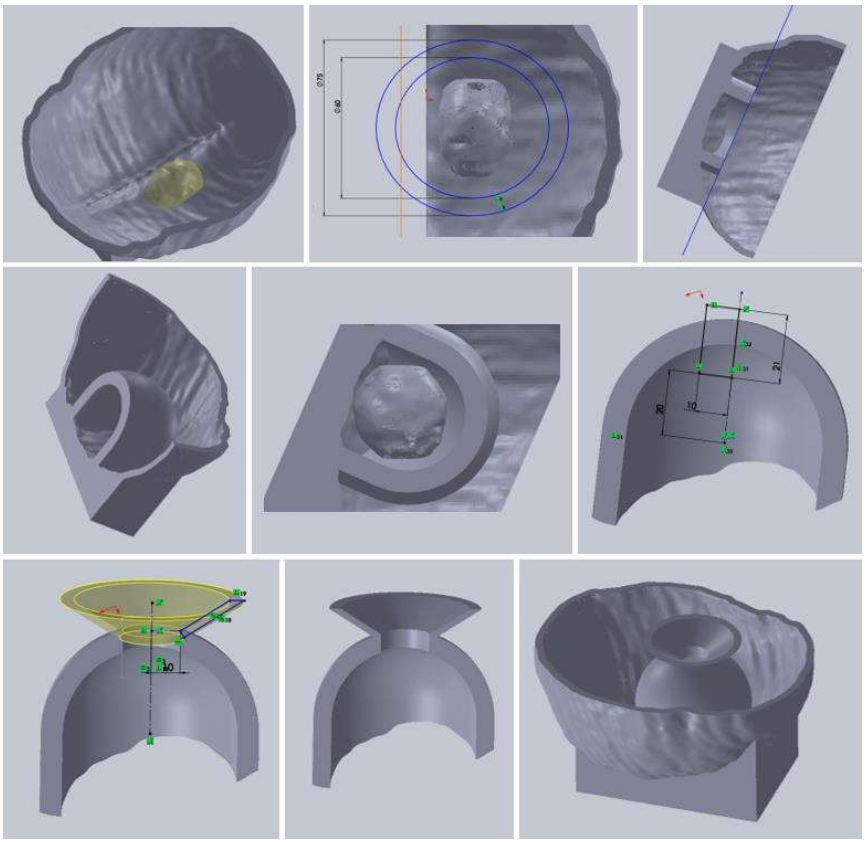

Figure 107. Design steps in SolidWorks to obtain the mold to define the working area.

With this mold that is located in the skull mold, it is possible to separate the different silicone mixtures. However, to guarantee the correct position of this mold during the pouring process, some tabs were added to be screwed in a support that will be placed on top of the brain mold (Figure 108).

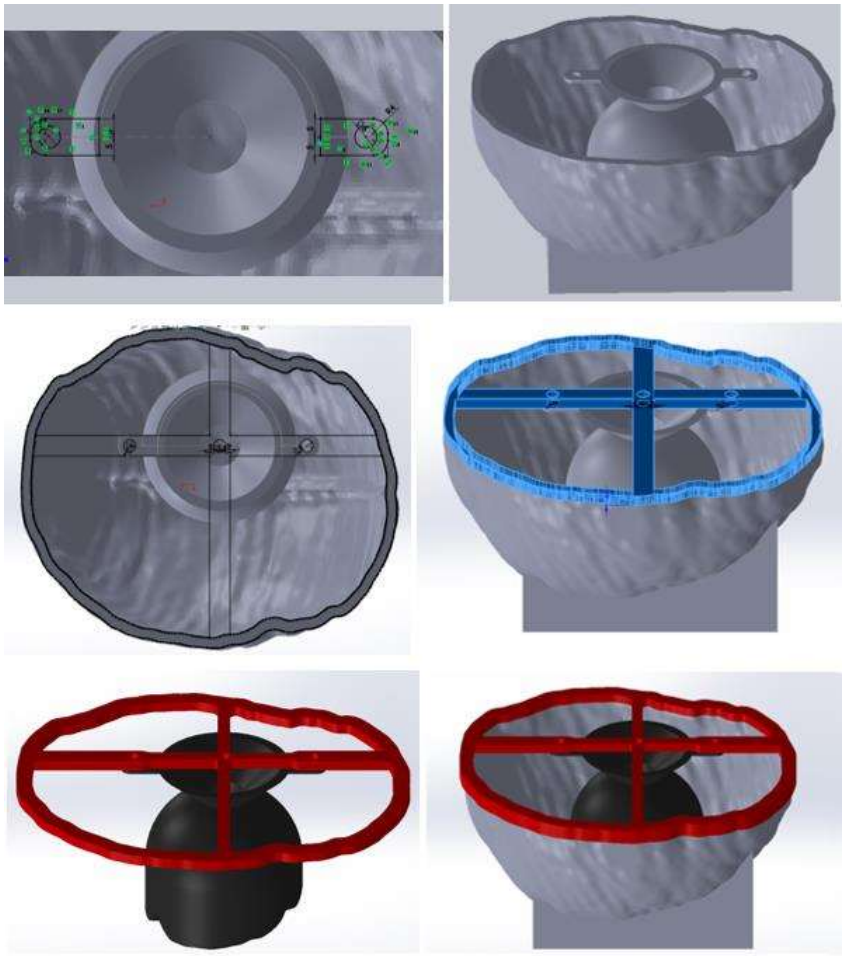

Figure 108. Design steps in SolidWorks to obtain the support (red) that is attached to the mold that defines the working area (black).

In order to keep the hematoma cavity, an insert with the segmented model of the tumor was designed to be placed inside the mold of the working area. This way, the soft silicone will fill the gap between the mold and the insert (Figure 109). Once cured the silicone, the insert will be removed thus leaving the cavity for the later infiltration of the simulated hematoma.

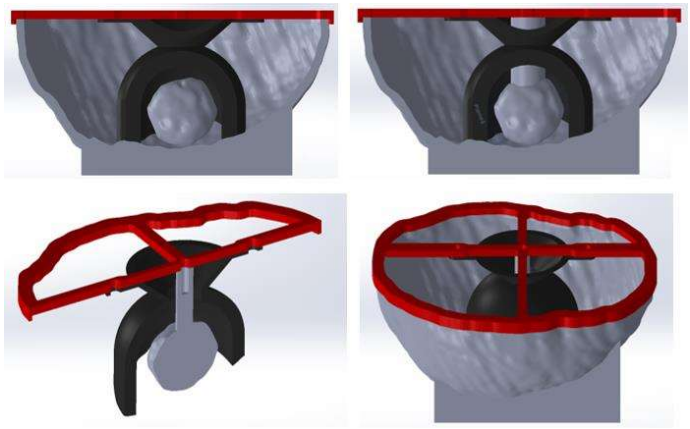

Figure 109. Design steps in SolidWorks to obtain the insert attached to the support (red).

These models were 3D printed with PLA (Figure 110).

Figure 110. Final 3D printed tools for the silicone pouring process.

Finally, an additional part (cone) was designed to be placed before the pouring of the final silicone (non-working silicone). This is a similar geometry to the tumor, but cut to reduce the demolding undercut. The objective of this part is to seal the cavity of the tumor during the pouring of the silicone of the non-working area (Figure 111).

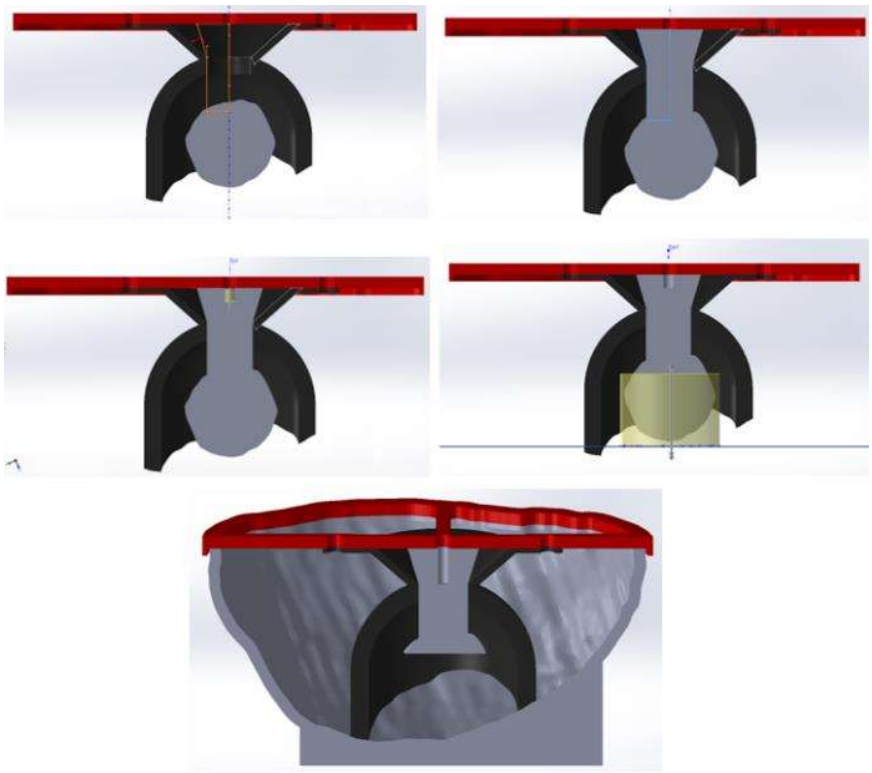

Figure 111. Design steps in SolidWorks to obtain the cone attached to support.

Once all the 3D printed models were obtained and 3D printed, the pouring process was carried out (Figure 112).

Figure 112. Brain model with the different silicone mixtures inside the skull model.

Although the initial idea was to first pour the silicone surrounding the tumor (the low consistency silicone, with Slacker component, for the working area), and then the rest (harder silicone for the non-working area), during the first trials it was observed that it was easier to do it the other way around. This means that the harder component (non-working area, outer part of the brain) should be poured before, and then the softest silicone surrounding the tumor (working area). This option was not initially considered to avoid undercuts in the demolding of the component that defines the working area. However, as the outer silicone has a high elasticity, this option was feasible and preferred to facilitate the poring process.

To do so, the mold to define the working area was designed as depicted in Figure 113. This part is fixed to the holder in the correct position and sealed in the bottom to the brain mold with modeling clay. The hardest silicone is then poured inside the mold and left to cure. Then, the mold defining the working area is removed and the insert with the geometry of the tumor is fixed to the holder and put inside the previously cured silicone. By using the available space between this part and the already cured silicone, the pouring of the working zone is accomplished. Finally, once the reticulation is finished, the mold defining the tumor is removed, once again taking advantage of the high

elasticity of the poured silicones, and the sodium alginate solution is injected into the remaining cavity.

As the sodium alginate solution that simulates the tumor may lose water over time, several tests were carried out to assess if this solution was stable once infiltrated in the simulated brain and covered with a silicone cap. The results showed good stability of the alginate solution, which means that this infiltration or filling process can be done during the preparation of the synthetic models and not necessarily just before the practical training.

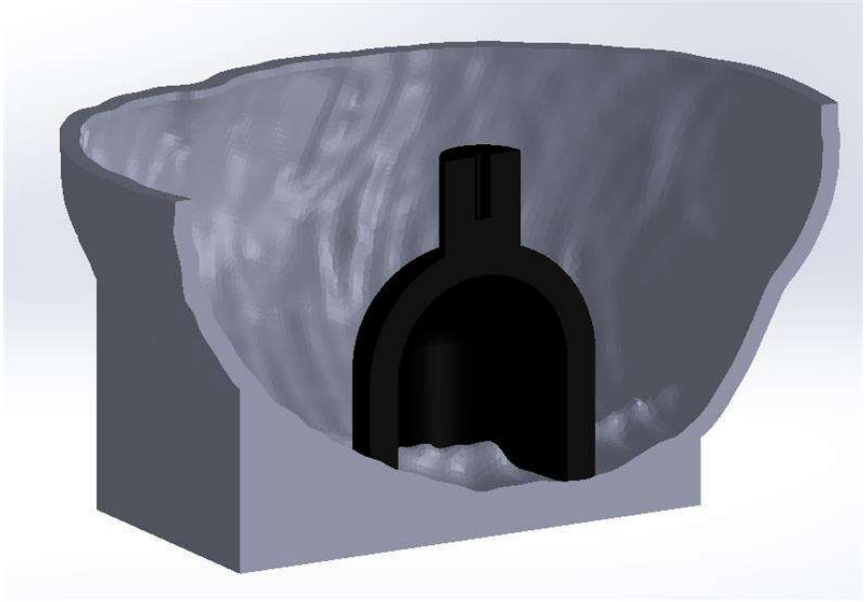

Figure 113. Design of the internal mold (black) to pour the hardest silicone and define the non-working zone. The upper part is fixed to the holder, which allows the correct positioning inside the brain mold.

Figure 114 shows the final molds and tools for the silicone pouring.

Figure 114. Brain mold with insert, holder and final design of the mold to define the working area.

Figure 115 shows the cured brain, already assembled in the skull and with the simulated tumor already infiltrated and covered with a cap.

Figure 115. Brain with tumor already infiltrated and assembled in the skull.

Figure 116 shows the final model with all the components (skull, brain with tumor inside, and base of the skull screwed).

Figure 116. Case 2 with skull and brain assembled (with tumor already infiltrated).

1.3. Training material for neurovascular surgery

The third summer school of the BrainIT project focused on neurovascular surgery. For this summer school, synthetic models of an aneurysm located in the medial cerebral artery (MCA aneurysm) were developed. As this document is being written before this summer school (August 2021), the current section shows all the design process and tests carried out so far, without having finished the complete manufacturing process.

1.3.1. Medial cerebral artery aneurysm

Synthetic models of a medial cerebral artery aneurysm was developed, starting from the real case depicted in Figure 117.

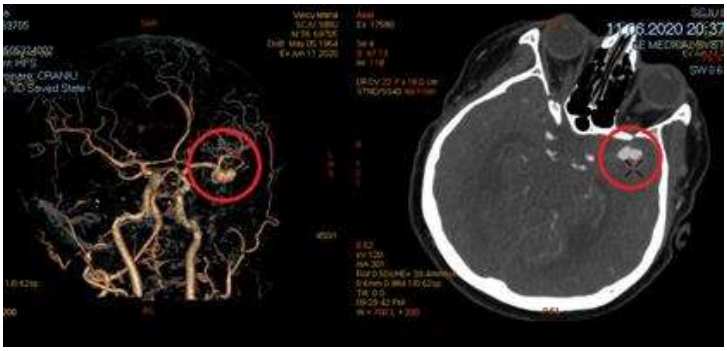

Figure 117. CT images of a real case of MCA aneurysm.

For the manufacture of blood vessels, the Digital Anatomy Printer (DAP) technology was selected, as it has a wide range of materials to mimic anatomy tissues. In order to choose the best material option and thickness of the vessels, 9 tube-shaped samples were manufactured and tested by neurosurgeons to find the best option to mimic real brain blood vessels for the surgery training. The external diameter was 3 mm (fixed value), while the internal diameter was modified with three different levels (1.8, 1.4 and 1 mm), so that the resulting minimum thickness was 0.6 mm, which is the minimum recommended thickness to guarantee the printability. For each geometry, three different hardness levels (compliance levels of 1, 3 and 6, being 1 the minimum 6 the maximum levels allowed) were used (vessel wall material, blood vessel family). Note that level 1 corresponds to the minimum hardness, and level 6 to the maximum hardness. Figure 118 shows the resulting 9 samples of the combination of the three internal diameters (or wall thicknesses) and the tree materials.

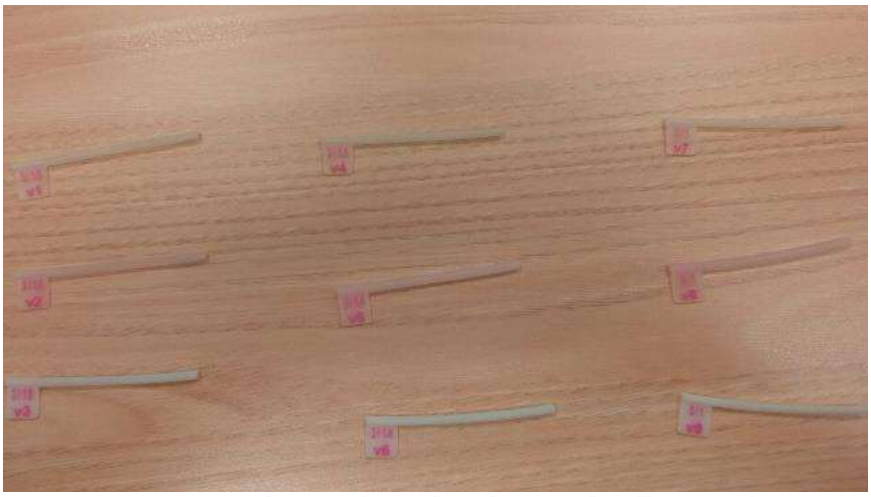

Figure 118. Tube samples with codes (vessel wall material).

Figure 119 shows the samples during the tests made by the neurosurgeons.

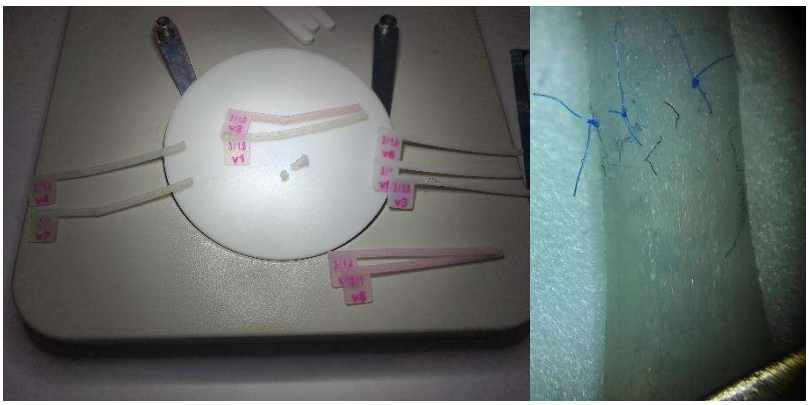

Figure 119. Tube samples during the tests. Left: general view. Right: view of sutures in the optical microscope.

Table 7 shows all the combinations with the corresponding code (from V1 to V9), diameters, materials, and also the neurosurgeons' score. According to the tests, the best combination was the one with the lowest wall thickness and the intermediate hardness (V2 option, with vessel wall thickness of 0.6 mm and slightly compliant hardness of the vessel wall material). This option provides a similar flexibility and fragile behavior to the real brain vessels.

Table 7. List of materials used for the samples.

Code	**D_{ext}/D_{int} (mm)**	**DAP material (hardness: 1-6)**	**Neurosurgeons' score (1-10) and comments**
V1	3/1.8	Compliant (1)	8
V2	3/1.8	Slightly compliant (3)	8.5
V3	3/1.8	Rigid (6)	Too hard and stiff
V4	3/1.4	Compliant (1)	6.5
V5	3/1.4	Slightly compliant (3)	6.5
V6	3/1.4	Rigid (6)	Too hard and stiff
V7	3/1	Compliant (1)	Too thick
V8	3/1	Slightly compliant (3)	Too thick
V9	3/1	Rigid (6)	Too hard and stiff

Once selected the material and thickness for the blood vessels, the 3D reconstruction was carried out by using the CT scan of the patient and processing the images in the ITK-SNAP software (segmentation process). In this case, the segmentation focused on the interior of the vessels (blood), which was obtained by removing the rest of material with the erase tool (Figure 120).

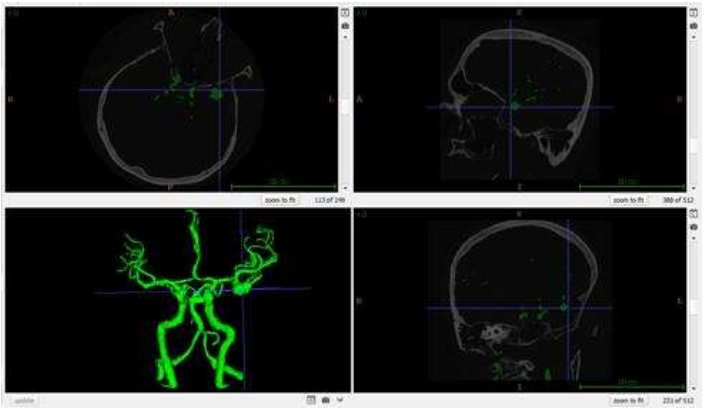

Figure 120. Segmentation of the interior of the blood vessel from the DICOM images.

Figure 121 shows the segmented model, where the aneurysm's area pecan be perfectly appreciated, as it was depicted in Figure 117.

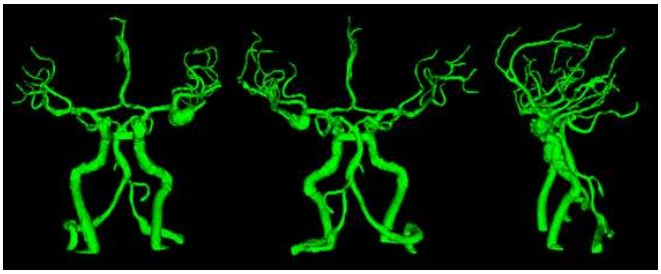

Figure 121. Different views of the 3D reconstruction of the interior of the vessels.

The STL file of the blood was imported into Meshmixer, where several operations were carried out to obtain the model of the hollow blood vessels, with a 0.6 mm thickness (Figure 122). Figure 123 shows the general dimensions of the final model.

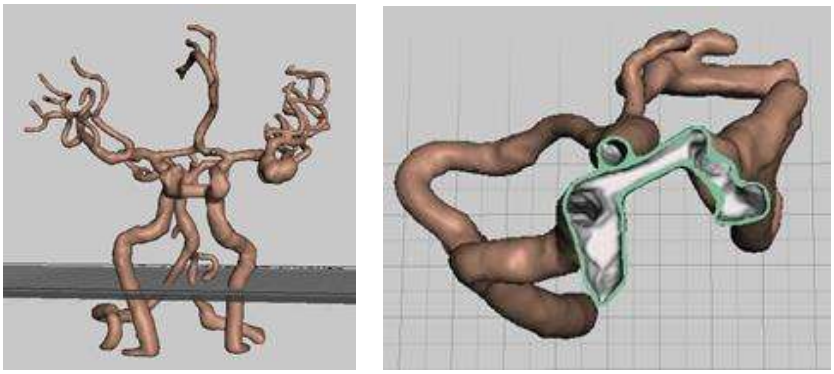

Figure 122. Blood vessels with 0.6 mm thickness. Left: general view. Right: section view (0.6mm wall thickness).

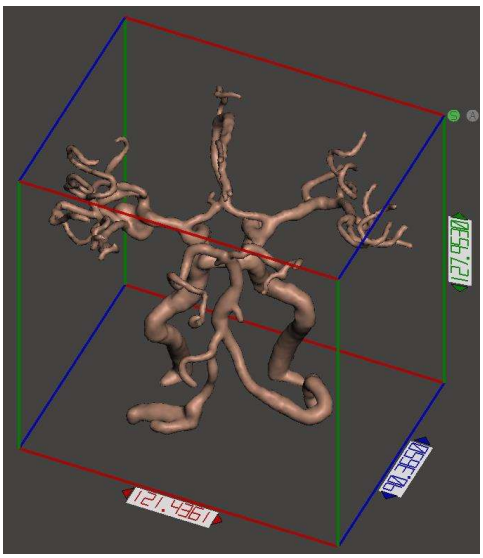

Figure 123. Dimensions of the blood vessels (approximately 121x90x128 mm).

On the other hand, in order to work with this model in the microscope, it must be cut to the region of interest (aneurysm zone) so that it can be fixed to the microscope and, at the same time, reduce the printing costs. As shown in Figure 124, the working area of the microscope corresponds to approximately 93 mm diameter if the fixation plate is used (external diameter) and 75 mm diameter if not (internal diameter). Similarly, the maximum available height from the bottom to the focal limit is 57 mm without the plate and 32 mm with the plate.

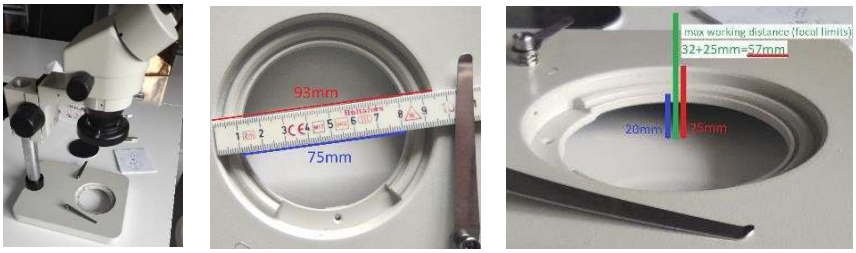

Figure 124. Optical microscope (left), dimensions of the working area (middle) and maximum heights (right).

Therefore, taking this into account, the cut was applied both to the model of the interior of the blood vessels and to the model of the blood vessels with a wall thickness of 0.6 mm. Both models were appended in the same document in Meshmixer to apply the same two plane cuts: the first on the left side and the second where the branches are located, thus reducing the model to a considerable size to be able to work with it in the microscope (Figure 125).

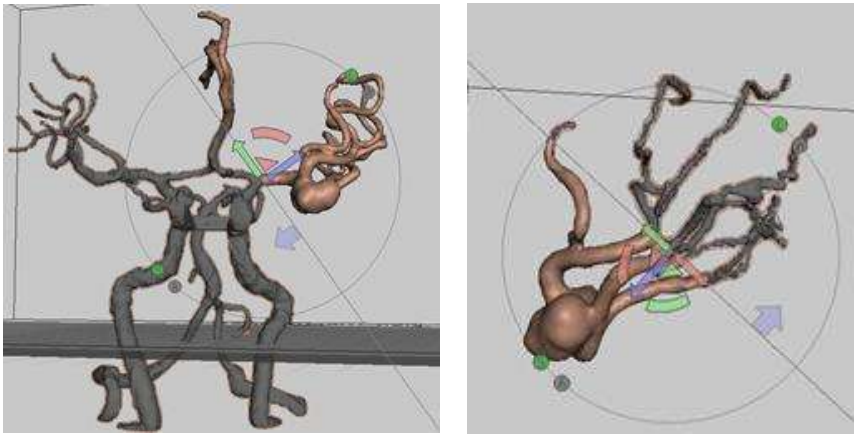

Figure 125. First plane cut to remove the lower part of the models (left) and second plane cut to eliminate the end of the vessels/blood (right).

Figure 126 shows the final models after the plane cuts (region of interest with the aneurysm). The dimensions of the reduced model were 31.8x31.8x37.9 mm, as depicted in Figure 127.

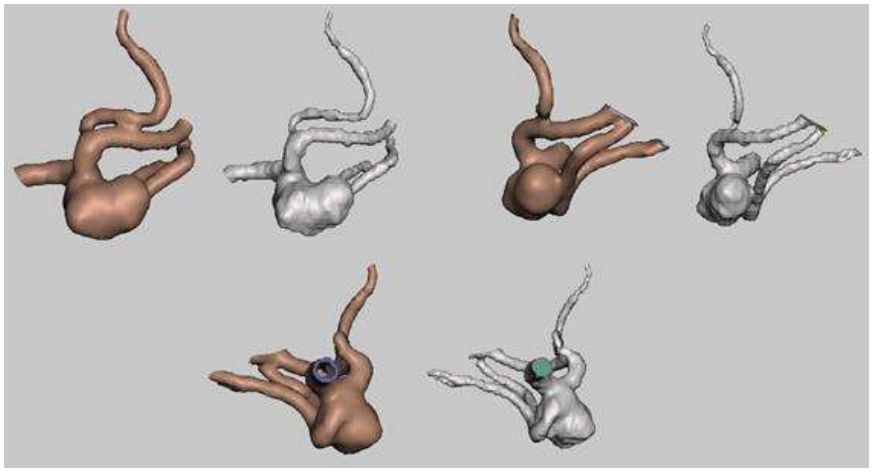

Figure 126. Reduced model of blood vessels and internal blood (in grey) seen from different angles.

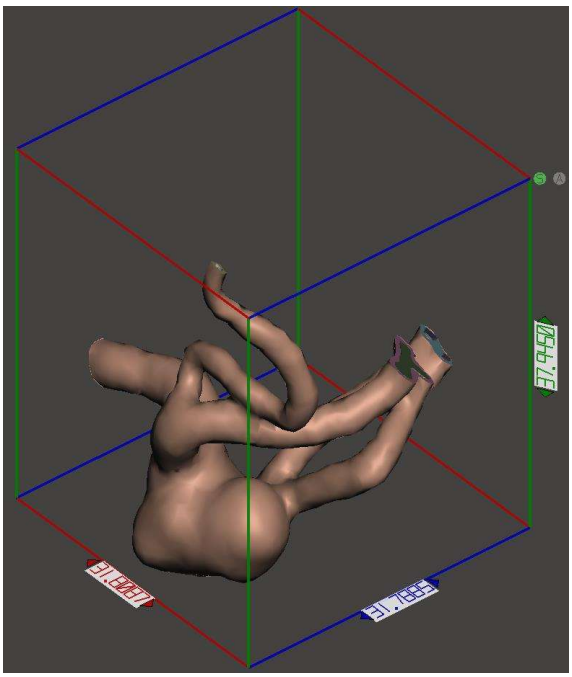

Figure 127. Dimensions of the reduced model of blood vessels and internal blood (in mm).

As the dimensions of the final reduced model do not exceed the dimensions of the working area of the microscope, the models can be properly placed and fixed in the microscope.

Once the segmentation and design of these models was carried out, 10 replicas of the reduced model and one replica of the complete vessels will be manufactured (process ongoing during the writing of this document). The complete model will serve as a reference to show all the vessels to the students, while the other 10 reduced blood vessels models will be the working models used by the trainees during the practical session. In both cases, the material to make the vessels will be the previously selected (V2 option, Table 7), and the support material that will be applied to the internal blood model will be GelMatrix. This material has a gel-like consistency that can be easily removed from the interior of the blood vessel models with water jet.

References:

1. R. P. Hubbard, "Flexure of layered cranial bone," *J. Biomech.*, vol. 4, no. 4, pp. 251–263, Jul. 1971.
2. C. Deck, S. Nicolle, and R. Willinger, "HUMAN HEAD FE MODELLING : IMPROVEMENT OF SKULL GEOMETRY AND BRAIN CONSTITUTIVE LAWS," 2004.
3. J. A. Motherway, P. Verschueren, G. Van Der Perre, J. Vander Sloten, and M. D. Gilchrist, "The mechanical properties of cranial bone," in *IFMBE Proceedings*, 2010, vol. 31 IFMBE, pp. 776–779.
4. R. Delille, D. Lesueur, P. Potier, P. Drazetic, and E. Markiewicz, "Experimental study of the bone behaviour of the human skull bone for the development of a physical head model," *Int. J. Crashworthiness*, vol. 12, no. 2, pp. 101–108, 2007.
5. J. E. Galford and J. H. McElhaney, "A viscoelastic study of scalp, brain, and dura," *J. Biomech.*, vol. 3, no. 2, pp. 211–221, 1970.
6. P. J. Basser, "Interstitial pressure, volume, and flow during infusion into brain tissue," *Microvasc. Res.*, vol. 44, no. 2, pp. 143–165, 1992.
7. Y. Tada, T. Nagashina, and M. Takada, "Biomechanics of Brain Tissue (Simulation of Cerebrospinal Fluid Flow)," *Trans. Japan Soc. Mech. Eng. Ser. A*, vol. 58, no. 551, pp. 1115–1121, 1992.
8. M. Kaczmarek, R. P. Subramaniam, and S. R. Neff, "The hydromechanics of hydrocephalus: Steady-state solutions for cylindrical geometry," *Bull. Math. Biol.*, vol. 59, no. 2, pp. 295–323, 1997.
9. M. Miga, K. Paulsen, F. Kennedy, J. Hoopes, A. Hartov, and D. Roberts, "Initial in-vivo analysis of 3D heterogeneous brain computations for model-updated image-guided neurosurgery," in *Lecture Notes in Computer Science (including subseries Lecture Notes in Artificial Intelligence and Lecture Notes in Bioinformatics)*, 1998, vol. 1496, pp. 743–752.
10. K. Miller, K. Chinzei, G. Orssengo, and P. Bednarz, "Mechanical properties of brain tissue in-vivo: Experiment and computer simulation," *J. Biomech.*, vol. 33, no. 11, pp. 1369–1376, Nov. 2000.
11. W. Goldsmith, "The state of head injury biomechanics: Past, present, and future: Part 1," *Critical Reviews in Biomedical Engineering*, vol. 29, no. 5–6. Begell House Inc., pp. 441–600, 2001.
12. Z. Taylor and K. Miller, "Reassessment of brain elasticity for analysis of biomechanisms of hydrocephalus," *J. Biomech.*, vol. 37, no. 8, pp. 1263–1269, Aug. 2004.